Sabine Innerhofer

Development of a Continuously Operated Tubular Crystallizer for the Production of Active Pharmaceutical Ingredients and Fine Chemicals

Entwicklung eines kontinuierlich betriebenen Rohrkristallisators zur Herstellung von pharmazeutischen Wirkstoffen und Feinchemikalien

DIPLOMA THESIS

Diplomarbeit zur Erlangung des akademischen Grades einer Diplom-Ingenieurin der Studienrichtung Verfahrenstechnik an der

Technischen Universität Graz

Advisors:

Univ.-Prof. Dipl.-Ing. Dr. techn. Johannes G. Khinast
Dipl.-Ing. Rafael J. P. Eder
Dipl.-Ing. Dr. techn. Heidrun Gruber-Wölfler

Institute for Process and Particle Engineering
Graz University of Technology

Graz, August 2010

STATUTORY DECLARATION

I declare that I have authored this thesis independently, that I have not used other than the declared sources / resources, and that I have explicitly marked all material which has been quoted either literally or by content from the used sources.

…… ……..

(date) (signature)

I. Danksagung

Danken möchte ich zuerst Prof. Khinast, der mir diese Arbeit ermöglicht hat. Mein Dank gilt auch den Mitarbeitern/-innen des Instituts für Prozess- und Partikeltechnik, im Besonderen meinen Betreuern Rafael und Heidi, ebenso wie Stefan, die alle meine Fragen stets geduldig beantworteten. Ebenso möchte ich mich bei Herrn Fischer und Markus bedanken, die mich im Labor hilfreich beim experimentellen Teil meiner Arbeit unterstützt haben.

Besonderer Dank gilt meiner Familie ohne deren Unterstützung mein Studium nicht möglich gewesen wäre. Bedanken möchte ich mich auch bei allen Freunden/-innen, Mitbewohnern/-innen und Kollegen/-innen, die mich während meines Studiums begleitet haben und mir stets mit ihrer Freundschaft und moralischen Unterstützung zur Seite standen und dadurch mein Leben in dieser Zeit sehr bereichert haben.

Sabine Innerhofer

II. Kurzfassung

Der entwickelte und getestete kontinuierlich betriebene Rohrkristallisator dient der Herstellung von Feinchemikalien mit Schwerpunkt pharmazeutische Wirkstoffe. Das Konzept des Reaktoraufbaus sah vor, Prozessparameter wie Reaktorlänge und Durchflussraten in einfacher Weise zu variieren sowie unterschiedliche Kühlabschnitte einzurichten. Im Kristallisator herrschten aufgrund des geringen Rohrinnendurchmessers von 2.0 mm ausgezeichnete Wärmeübergangsbedingungen, die eine herausragende Prozesskontrolle gewährleisteten. Als Modellsubstanz wurde Acetylsalicylsäure (ASA) aus Ethanol (EtOH) kristallisiert. Eine mit Keimkristallen beladene ASA-EtOH-Suspension wurde in den Reaktor gefördert und mit einer erhitzen, leicht untersättigten ASA-EtOH-Lösung vermischt. Die Kontrolle der Übersättigung erfolgte durch die Konzentration der Lösungen, die Keimbeladung und die Temperaturgradienten. Während des Kristallisationsprozesses wuchsen die Keimkristalle, die eingesetzt wurden, um unkontrollierte Keimbildung zu verhindern. Der Kristallisator konnte erfolgreich unter allen getesteten Prozessbedingungen betrieben werden.

Zwei verschiedene Serien von Experimenten wurden durchgeführt, um den Kristallisator zu testen. Die Durchflussrate und Reaktorlänge wurden jeweils variiert, während die anderen Einstellungen unverändert blieben. Der Reaktor wurde entweder mittels eines Wasserbades auf konstanter Temperatur (30°C) gehalten oder mit Luft gekühlt (21°C), auch wurden verschiedene Kühlstufen angewandt (bis zu 0°C). Unterschiedliche Reaktorlängen ergaben weder eine signifikante Änderung der Kristallkorngrößen noch der Produktausbeute. Höhere Durchflussraten reduzierten die Agglomeratbildung wodurch kleinere Partikeldurchmesser erzielt wurden, die Produktmasse jedoch unverändert blieb. Die Produktausbeute wurde erheblich erhöht durch die Anwendung von Luftkühlung im Gegensatz zur Prozessführung mit konstanter Temperatur von 30°C. Durch intensives Kühlen mittels mehrerer Kühlschritte konnte die Ausbeute noch weiter gesteigert werden.

III. Abstract

A continuously operated tubular crystallizer for the production of fine chemicals with focus on active pharmaceutical ingredients (APIs) was developed and tested. The reactor set-up was designed to easily vary process parameters like reactor length and flow rates and to apply different cooling segments. Due to an inner diameter of 2.0 mm excellent heat transfer conditions prevailed, granting outstanding process control. Acetylsalicylic acid (ASA) was crystallized from ethanol (EtOH) as model substance. A seeded ethanolic suspension was fed into the reactor and mixed with a heated, slightly undersaturated ASA-EtOH solution. Supersaturation was controlled through the concentration of the solutions, seed load, and cooling gradients. Seed particles were introduces to avoid uncontrolled primary nucleation and grew during the crystallization process. The crystallizer was successfully operated for all process conditions tested.

Two different series of experiments were conducted to test the system. Flow rate and reactor length were altered while keeping all other process parameters constant. The reactor was either kept at constant temperature using a water bath (30°C) or cooled through air convection (21°C). Furthermore different cooling gradients were applied (up to 0°C). For varying reactor lengths no significant changes of either crystal size or product yield was observed. Higher flow rates resulted in smaller average number mean diameters (NMD) due to reduced agglomeration effects, though the product mass remained the same. The product yield was increased considerably by applying air cooling compared to process control with constant temperature of 30°C. Intense cooling due to different cooling segments with a reactor end temperature of 0°C resulted in further increase of the yield.

IV. Table of Contents

V. List of Figures

VI. List of Tables

VII. Abbreviations

API	Active pharmaceutical ingredient
AR	Aspect ratio
ASA	Acetylsalicylic acid
cGMP	Current good manufacturing practice
CSD	Crystal size distribution
DTB	Draft tube baffled
EtOH	Ethanol
Exp S1	Experimental series 1
Exp S2	Experimental series 2
F1	Feed flow of solution 1
F2	Feed flow of suspension 2
FB	Fluidized bed
FC	Forced circulation
I1	Inlet (storage vessel) of solution 1
I2	Inlet (storage vessel) of suspension 2
log-NV	Logarithmic normal value
MSMPR	Mixed suspension mixed product removal
NMD	Number mean diameter
No.	Number
P I	Pump I
P II	Pump II
PAT	Process analytical technology
PP	Polypropylene
PSD	Particle size distribution
PTFE	Polytetrafluoroethylene
QbD	Quality by Design
r.T.	Room temperature
STR	Stirred tank reactor

VIII. Nomenclature

A	$[m^2]$	Reactor cross section area
A_m	$[m^2]$	Mean tube surface area
A_n	$[m^2]$	Nucleus surface
AR	[-]	Aspect ratio
c	[g/mol]	Concentration
c*	[g/mol]	Saturation concentration
c_p	[J/(kgK)]	Specific heat capacity
Δc	$[mol/m^3]$	Supersaturation
d_i	[m]	Inner diameter
d_o	[m]	Outer diameter
d_p	[m]	Particle diameter
$\overline{d_p}$	[m]	Number mean diameter
$d_{p,50}$	[m]	Volume median diameter
G	[J/mol]	Gibbs free energy
Δh_{cryst}	[J/kg]	Heat of crystallization
k	$[W/(m^2K)]$	Thermal transition coefficient
L	[m]	Nucleus size
L*	[m]	Critical nucleus size
L_R	[m]	Reactor Length
m_i	[kg]	Mass of component i
$\dot{m}_i$	[kg/s]	Mass flow of component i
Δm	[kg]	Mass gain (yield)
N_1, N_2, N_3	[-]	Nyvlt coefficients
n_i	[mol/s]	Mole flow of component i
Nu	[-]	Nußelt number
Pr	[-]	Prandtl number
Q	[W]	Heat flow
$q_r(x)$	[1/m]	Frequency distribution
$\Delta Q_r(x)$	[-]	Relative frequency of particles

R	[J/molK]	Ideal gas constant
Re	[-]	Reynolds number
R_W	[K/W]	Thermal resistivity of tube
s	[µm]	Standard deviation of NMD
S	[-]	Supersaturation ratio
T	[K]	Temperature
t	[s]	Time
t_{res}	[s]	Residence time
u	[m/s]	Flow velocity
$\dot{V}$	[m^3/s]	Volume flow
V_R	[m^3]	Reactor volume
V_n	[m^3]	Nucleus volume
V_x	[m^3]	Particle volume
w_i	[kg/kg]	Mass fraction of component i
x_i	[mol/mol]	Molar fraction of component i
Δx	[m]	Particle class range

α	[W/(m^2K)]	Heat transfer coefficient
γ_{CL}	[J/m^2]	Interfacial tension
η	[Pas]	Dynamic viscosity
λ	[W/(mK)]	Heat conductivity
ρ	[kg/m^3]	Density
σ	[-]	Standard deviation of log-NV
Ψ	[-]	Sphericity of Wadell

1. Goals and Motivation

The objective of this work was to develop and test a continuously operated crystallizer for the crystallization of fine chemicals with focus on active pharmaceutical ingredients (APIs). The goal was to develop an easy to handle and alterable device that allowed fast and unproblematic changes of the process parameters. Defined growth and control of the crystal size distribution (CSD) were set as main target to ensure a robust and reproducible process featuring constant product quality.

The main focus of this work was to assay the influence of single parameters on the crystallization process in a tubular reactor. The system had to be tested for a model substance for varying flow rates, reactor lengths and cooling gradients. A reactor concept and an operating method had to be developed, and an analytical method and an evaluation tool had to be realized.

2. Introduction

In this chapter some general crystallization issues and production methods are discussed to impart basic knowledge and understanding of the choices made for the reactor design and experimental set-up, and the conclusions drawn from the test results.

2.1. Active Pharmaceutical Ingredient Production

Pharmaceutical products consist of a biologically active pharmaceutical substance and excipients. Particles of both active and inactive ingredients exist as dry powders, liquid and semisolid dispersions [1]. The production of pharmaceutical substances requires reproducibility and consistency of the solid state properties [2]. Physical and chemical stability is essential to ensure constant drug properties and release. The particle size, the particle size distribution (PSD), and also the shape of the particles have an influence on the bioavailability, processability, and quality attributes [3].

The size of the particles can vary from the nanometer to the millimeter scale and depends on the route of administration and the dosage form. The common particle size for APIs for oral administration ranges from 100-200 µm because compaction behavior and powder flow properties of this size are favorable for direct-compression tablets [1]. Drugs designed for pulmonary delivery have particle sizes of 1-5 µm. Small particles dissolve faster and offer a better bioavailability but are more difficult to handle during the manufacturing process. Additionally, the PSD affects the handling of the product, such as filtration, drying and formulation. It has an impact on process attributes like flow, compactibility, sticking, and segregation that influence tablet strength and uniformity of the content [4]. Solution temperature, supersaturation, solvent type, impurities, and additive concentration, in combination with the crystal structure, affect the particle shape. The particle shape in turn affects the dissolution behavior and crystal growth, and also processing properties and therefore product quality.

Procedures to implement novel technologies in the pharmaceutical industry are well regulated. To ensure quality in both manufacture and testing binding guidelines as current good manufacturing practices (cGMP) are imposed. Quality by design (QbD) concepts aim at better process understanding and identification of possible risks involved, and thus improving the manufacturing process of the product. Novel process analytical technologies (PAT) focus on implementing enhanced analytical methods for process monitoring and control [2-5].

2.2. Continuous Processing

Although continuous processing is quite common in other manufacturing industries, batch processes are common standard within the production of pharmaceutical products [5]. Depending on the application, continuous processing can offer technical and economic benefits compared to batch manufacturing. Main advantages are better process control and easier scale-up [2].

For applications with very small production rates or where losses of the material have to be avoided, batch crystallization is often applied. When the material is cooled through a wide temperature range or the final temperature requires very high vacuum, batch production is in general more economical than multiple stage continuous production [6]. However, batch crystallization usually involves a complex combination of growth, secondary nucleation, agglomeration, and particle breakage. Different batch runs yield product variations because the quantity of initial nuclei is difficult to control. The mixing behavior has great influence on this since insufficient agitation can cause local supersaturation spots, while excessive stirring can lead to particle breakage and secondary nucleation. Scale-up of stirred-tank reactors is difficult and often results in significant changes in both PSD and crystal morphology [4]. Batch handling of wet or semidry product also presents difficulties.

Due to their complexity, batch processes are often not well understood and optimized [5]. Unlike batch processes, in continuously operated devices, steady state conditions prevail that are easier to understand and handle. Continuous production demands smaller operating devices and smaller storage facilities compared to batch production. This comes

with the advantage of a better heat transfer because of an increased specific area per volume and often features plug flow conditions. Processing dangerous and also highly exothermic reactions in small devices minimizes safety risks and allows significantly shorter operating times. Because of the reduced size of the equipment and the operating mode, the amount of solvents used in continuous processing systems is far less, and in addition recycle flows can be implemented [7]. Milling and recrystallization are common downstream operations in the pharmaceutical industry because batch production often generates crystals that have different specifications than the desired product [8]. Continuous processing enables narrower CSDs and fewer waste product, hence production steps can be reduced and production time shortened. From an economical point of view, continuous processing is favorable as well. Smaller operating devices and storage facilities minimize investment costs. Reduction of solvent and energy consume, waste material generation, avoiding down time for filling and maintenance, and automation of production steps decrease production costs [7].

Nevertheless, there also exist some drawbacks for continuous processing. A continuous production plant is less flexible than a batch set-up regarding variations of the raw material or changing product requirements, and therefore usually only pays off if the given conditions are quite steady and a certain amount of product is required. Start-ups and shutdowns caused by equipment failure or other operational issues present challenges in product homogeneity for continuous production [5].

The current trend in the pharmaceutical industry is mainly not to change existing batch operations to continuous processes, but to develop new production methods that lead to novel technologies [5]. A highly promising approach is microreaction technology [9-11]. It offers excellent process conditions due to exceptional heat transfer control and online data monitoring. A major advantage of this technology is the simple transition from experimental phase to pilot plant and production stage by numbering-up. However, the application for crystallization processes is still limited. The small channels are prone to plugging and create practical limitations on the size of the particles that can be produced [4]. To date most applications for microreaction technology aim at the production of inorganic nanoparticles, but research has been done also in the field of organic nanoparticles [12-14]. Publications discussing the development in microreactor technology and its implementation in pharmaceutical and chemical syntheses like [15],[16] constantly increase in number.

2.3. Fundamentals of Crystallization

Crystallization is an important separation and purification process in the pharmaceutical and fine chemical industry [17]. Very high purity products can be produced from impure solutions. The energy input required for this unit operation is quite low compared to other common separation methods, such as distillation, and so are operating costs [6].

2.3.1. Solubility and Saturation

Solubility is a material property that describes the ability of a chemical substance to dissolve in a liquid solvent and form a homogeneous solution. The solubility of materials depends on temperature, pressure and the presence of other substances in the solvent. For most materials it declines with declining temperature.

The saturation concentration describes the maximum amount of solute that is soluble in the solvent. If the amount of solute present in the solution exceeds the saturation concentration, the solution is supersaturated. A solution can be supersaturated up to a maximum amount before it becomes unstable. This upper boundary is called the spinodal curve. The zone between the saturation curve and the spinodal curve is known as the metastable zone (see Figure 1), crystallization usually occurs in this range.

A supersaturated solution is not in equilibrium. To achieve thermodynamic equilibrium crystallization takes place. Once first crystals are formed both nucleation and crystal growth decrease supersaturation. With an activity coefficient γ = 1 supersaturation Δc can be expressed as the difference of actual concentration c to saturation concentration c*. The supersaturation ratio S is the ratio of concentration to saturation concentration.

$$S = \frac{c}{c^*} \tag{2.1}$$

$$\Delta c = c - c^* = S - 1 \tag{2.2}$$

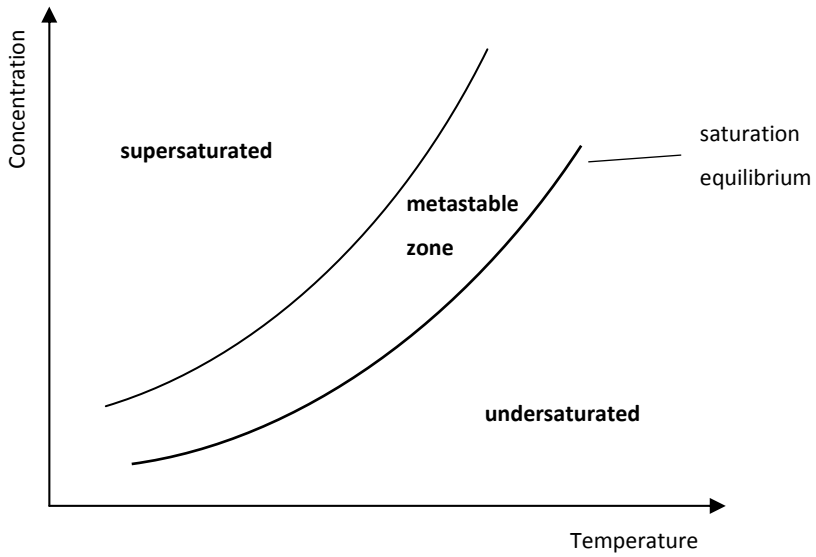

Figure 1: Saturation and metastable zone (adapted from [17])

Typically, a crystallizer is operated at low supersaturation because high supersaturation usually means the formation of small crystals (fines) that pose a common problem for subsequent processing steps (e.g. filtration).

There are four main methods to create supersaturation. Supersaturation can be created by cooling, evaporation of solvent, chemical reaction, and change of solvent composition (e.g. drowning-out). As the solubility of most materials declines with declining temperature, cooling is a common method used to create supersaturation. Cooling can be achieved with an external jacket or a cooler inside the crystallizer. In continuous crystallization processes the main goal is to maintain an optimum supersaturation to keep the growth rate high, while keeping the rate of nucleation low. In batch operated devices a constant cooling rate is usually applied as a simple operating method. A better approach is to set the cooling rate so that the supersaturation is kept constant during the cooling process. Otherwise, because of the small seed surface available at the beginning, very high supersaturation will be created, leading to extensive nucleation and slow crystal growth towards the end because of low supersaturation [18]. If the solubility of the material does not change significantly at lower temperatures, evaporation can be used to create supersaturation. This method applies especially for nonaqueous solvents with relatively high vapor pressures. The solution is heated to the boiling point of the solvent so that it evaporates and the solute crystallizes. Vacuum crystallization combines cooling and evaporative crystallization. The solution is

cooled and evaporated simultaneously by decreasing pressure and temperature. Inorganic salts can be crystallized from aqueous solutions by adding organic substances and evaporating the drowning-out agents after the crystallization. Energy consumption for drowning-out crystallization is quite low because of the usually low evaporating enthalpy of the agents. Generating supersaturation through chemical reaction is known as precipitation. Two soluble materials react with each other and form a product with lower solubility. Generally, this is a very rapid process in which a large number of nuclei form.

In most cases different methods can be applied. To choose the most adequate method, the system equipment available, solubility versus temperature, and the production rate required should be evaluated.

2.3.2. Nucleation

Crystals are created when nuclei form and grow. If there are no crystals or foreign particles present in the solution, homogeneous nucleation takes place.

Supersaturation does not necessarily result in crystallization. When the solubility of a solution is exceeded, cluster of molecules form. When the critical size for crystal creation L* is not reached, the total Gibbs energy ΔG is positive and will cause the cluster to dissolve again (see Figure 2). Clusters above the critical size can continue growing into crystals. The free energy change is the sum of the free energy change ΔG_V for the phase transformation (negative quantity) and the free energy change ΔG_A for the formation of the nucleus surface (positive quantity).

The change in positive free surface energy ΔG_A increases with the interfacial tension γ_{CL} between the solid crystal surface and the surrounding solution as well as with the surface of the nucleus A_n. The change in free volume energy ΔG_V depends on the nucleus volume V_n, the concentration c_c and the energy $RTln\frac{c}{c^*}$ for an ideal system (R= gas constant, $\frac{c}{c^*}$= supersaturation ratio).

$$\Delta G = \Delta G_A + \Delta G_V = A_n\gamma_{CL} + \left(-V_n c_c RTln\frac{c}{c^*}\right) \quad (2.3)$$

A thermodynamically stable nucleus exists when the total free energy ΔG does not change when elementary units are added or removed.

$$\frac{\partial \Delta G}{\partial L} = 0 \tag{2.4}$$

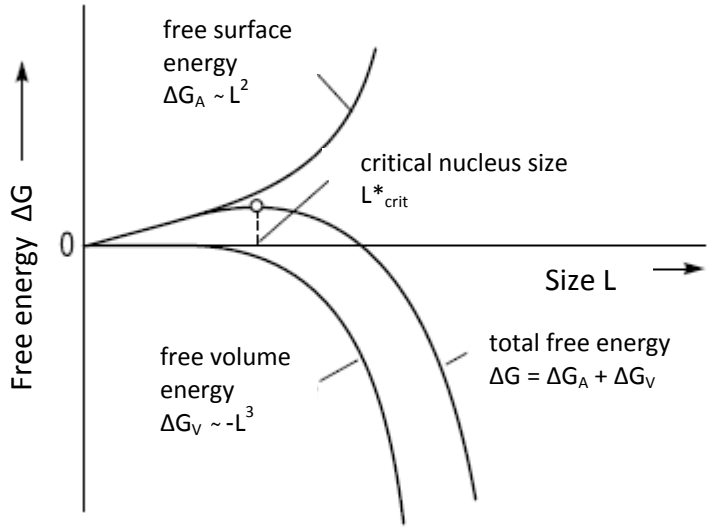

Figure 2: Free energy against nucleus size (adapted from [18])

Nucleation in the presence of foreign particles is known as heterogeneous nucleation. In general, if nucleation occurs in absence of crystals it is known as primary nucleation. Secondary nucleation occurs due to attrition caused by collision contact with other particles or the surroundings and due to shear stress. Microstructure and roughness of the parent crystal surface play a role, and are also influenced by supersaturation.

2.3.3. Crystal Growth

In order to grow, elementary units have first to be transported through convection and diffusion through the bulk towards the crystal, and then be integrated into the lattice. Depending on substances, flow conditions and supersaturation, either diffusion or integration can be the limiting step for the growth kinetics. For diffusion-controlled crystal

growth, the integration velocity is very high compared to the diffusion rate for the mass transport in the interface from the bulk towards the crystal. If the mass transfer coefficient is very high, the crystal growth is controlled by integration and depends on the surface roughness, lattice dislocations, and if impurities or additives adsorb onto it.

In a crystallization process both nucleation and crystal growth occur. When supersaturation is near or greater the upper limit of the metastable region, in general nucleation is the dominant process. A low supersaturation level and the presence of sufficient crystal surface area will favor crystal growth. The seed amount, the shape and size of the seeds, the size distribution and other factors also have a strong influence on what process dominates. To control a crystallization process, knowledge of both nucleation and growth processes is necessary.

In a nucleation-driven process, usually fine crystals with a wide crystal size distribution (CSD), high surface area and low bulk density prevail, posing a problem for filtration and drying steps and making scale up difficult. A growth dominated process has the advantages of a larger average particle size that comes along with lower surface area, higher bulk density, and therefore improved mixing behavior and processability. Impurities can have a strong effect on growth by retarding it (slowing it down) or even inhibiting it. On the other side, impurities can suppress nucleation and therefore enhance growth.

Nucleation is kinetically favored compared to crystal growth. However, small particles have a larger surface to volume ratio than larger particles. Molecules on the surface are less stable as if already fully integrated into the bulk and therefore larger particles are thermodynamically favored. Over time, larger particles continue to grow at the expense of smaller ones that continuously shrink and slowly disappear. This phenomenon is called Ostwald ripening.

The nucleation to crystal growth ratio is important for industrial crystallization processes because growth controls the product crystal size and size distribution [6].

2.3.4. Crystal Morphology and Structure

Crystals consist of a three-dimensional periodic assembling of elementary modules consisting of atoms, ions or molecules. The shape is determined by the type of lattice and the interfacial surface.

Factors influencing the crystal shape are the solvent, temperature, supersaturation rate, additives and impurities. The shape depends on the growth rate of each face, the presence of impurities or additives on certain faces that reduce or inhibit crystal growth, and the intensity of agglomeration and attrition. According to size and shape, particles have different characteristics and individual processing qualities. Crystals close to spheres show better flowability than needle or plate like particles and are therefore preferred in the manufacturing process.

2.3.5. Agglomeration and Aggregation

If particles merge with no supersaturation present it is called aggregation. Agglomeration occurs in a supersaturated solution when aggregated crystals coalesce.

Agglomeration can be a consequence of collision of nuclei. The bonding is affected by surface chemistry and hydrodynamics. Agglomeration is usually undesired because solvent or impurity entrapments might occur, forming less stable crystals that are prone to break in subsequent processing steps, and eventually lead to unwanted changes in the CSD. At very high supersaturation levels, stronger agglomerates form that are less likely to break in downstream processes. To reduce agglomeration, supersaturation and nucleation has to be controlled and the mixing performance has to be adapted.

One way to reduce or suppress agglomeration is the use of additives. However for pharmaceutical production they are usually not applied because of regulatory reasons [6]. In some cases directed agglomeration is favored, e.g. in granulation processes.

2.3.6. Attrition

Attrition occurs due to crystal-crystal contact or by contact of crystals with the impeller, the vessel or tube walls. Due to the impact small crystal fragments are formed that have the

same functionality as seed particles. This occurs especially during crystallization processes with a mean particle size larger than 100 µm. Smaller particles tend to follow the fluidic flow and therefore cause lesser collisions. In systems with a mean particle size smaller than 100 µm heterogeneous nucleation is more likely due to less attrition and because it requires less energy than primary nucleation [19].

Figure 3 shows the influence supersaturation has on the mean particle size and how attrition and agglomeration can affect the outcome.

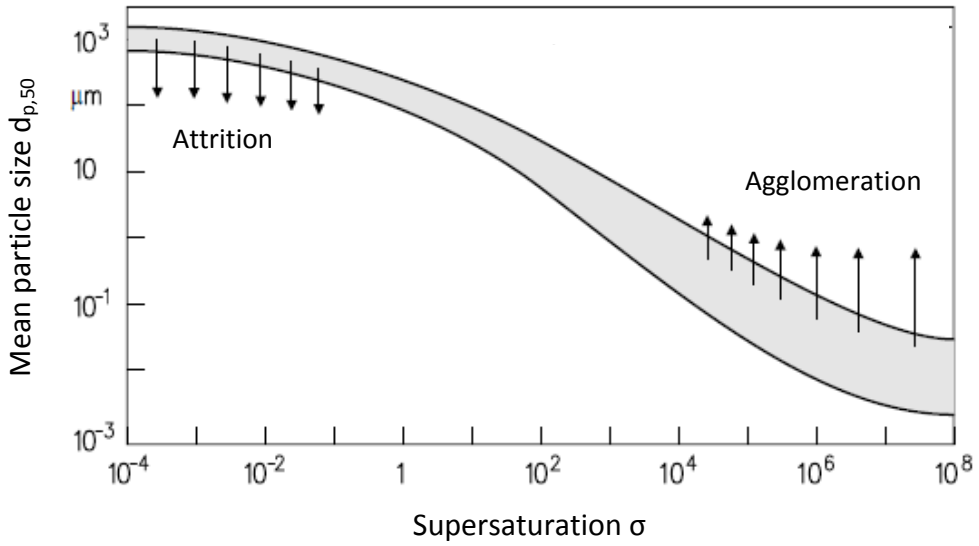

Figure 3: Influence of attrition and agglomeration on the mean particle size (adapted from [19])

2.3.7. Seeding

Spontaneous nucleation is difficult to control because it depends on local conditions in the crystallizer, like supersaturation rate and mixing. Impurities can also result in unintentional seeding. Seed crystals are introduced to control the quantity of particles and the PSD. However, the final outcome strongly depends on the amount of seed particles applied and the supersaturation rate. When low level seeding is applied, larger particles form that are more likely to induce secondary nucleation. A high amount of seeds combined with low supersaturation is most likely to result in a successful growth of seeds. When seeds are added to a solution that is still undersaturated, dissolution and reduction of some seed

particles occur. When seeds are added after the solution reached saturation, this might also induce nucleation [18].

2.3.8. Mixing

Impeller speed and type influence the circulation and local turbulences. Increased mixing improves the heat transfer by increasing the bulk turnover and the uniformity of the suspension by counteracting settling. High energy input due to fast mixing enhances primary nucleation, especially during reaction crystallization, but can also lead to particle breakage and increased secondary nucleation. Keeping all crystallization parameters constant upon scale-up is hardly achievable because of the complexity of the factors [17].

2.4. Crystallization Apparatus

The selection and design of a crystallizer depends on the rate of supersaturation to be produced, the mode of operation, the desired CSD and median crystal size, and the purity of the product [18]. A distinction between crystallization from solution and crystallization from melt has to be made. Cooling-type crystallizers are commonly used to crystallize material with a steep solubility progression (e.g. hydrated salts). They permit high overall yields and reduce the energy requirements of the separation process. If the material has a low solubility, surface cooling, evaporation cooling, or constant temperature evaporation are applicable.

Some continuously operated industrial crystallizers are shown in Figure 4. The design of the crystallizers can vary as different flow cycles and classifying options are possible. Depending on the type of crystallizer, the cooling can occur through an external heat exchanger or inside the crystallizer. a) The stirred tank reactor (STR) is also called draft tube baffle (DTB) crystallizer when a draft tube is implemented to direct the liquid flow and minimize the specific power input of the crystallizer. An impeller provides the mixing of the solution and keeps the crystals in suspension. b) The fluidized-bed (FB) crystallizer, also called Oslo

crystallizer, is a classifying crystallizer. It features a crystal bed, which is fluidized by a supersaturated solution. The suspension flow is conducted by a circulating pump keeping the crystals in suspension without contact by a stirring device. The crystals produced have a narrow CSD and are generally coarser than from stirred vessels or forced-circulation (FC) crystallizers. A FB crystallizer requires a large crystallizer volume and high investment costs while operating costs are low. c) In forced-circulation (FC) or mixed suspension mixed product removal (MSMPR) crystallizers the suspension is circulated in a loop by a pump, causing secondary nucleation and particle breakage. Usually, FC crystallizers are used for high evaporation rates and operated at low vacuum or atmospheric pressure.

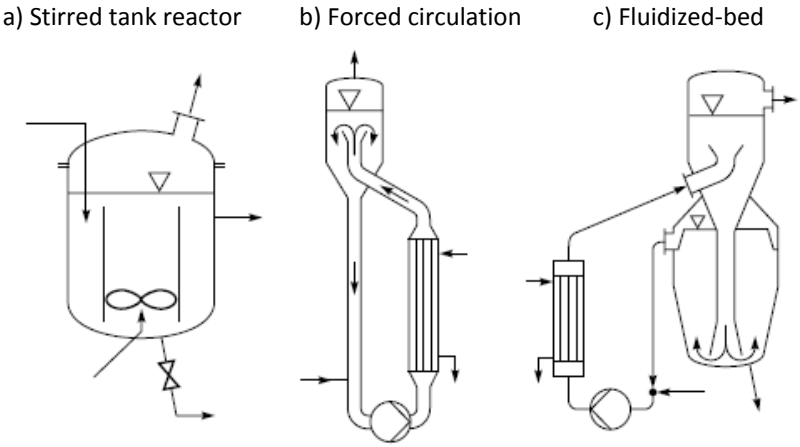

Figure 4: Typical continuously operated industrial crystallizers (ref. [18])

To achieve the best result in a crystallizer the optimum supersaturation should occur evenly all through the growth zone, the solution should be perfectly mixed, and all crystals should be in suspension [18]. The advantage of a tubular crystallizer with a small inner diameter is that plug flow conditions prevail and no segregation occurs. The crystallizer discussed in this work features a heat exchange surface throughout the entire tube length and therefore allows excellent temperature control at any time of the process. Superior control of the process conditions (e.g. supersaturation rate) provides selected crystal growth of the seed particles, a narrow CSD, and short residence time of the crystals.

3. Experimental Approach

In this work the parameters that have an influence on the crystallization process in a tubular reactor were investigated. The goal was to design a flexible reactor concept for continuous processing, do an experimental evaluation of the reactor by using a model substance, and elaborate a robust operating method and a simple evaluation tool. Supersaturation was intended to be created by cooling. The introduction and controlled growth of seed particles was of major interest.

The crystallization of ASA from an ASA-EtOH solution was chosen as test system. Both components are non-toxic and commercially available. ASA easily dissolves in EtOH, and data about the solubility can be found in literature [20].

Figure 5 shows a schematic of the functional principle of the seeded tubular crystallizer presented in this work. An ASA-EtOH solution (1) is fed to the reactor and mixed with a seeded ASA-EtOH suspension (2). The supersaturation is controlled by regulating the temperature of the suspension by applying or deducting heat (Q) along the reactor tube, causing the seed crystals to grow inside the crystallizer.

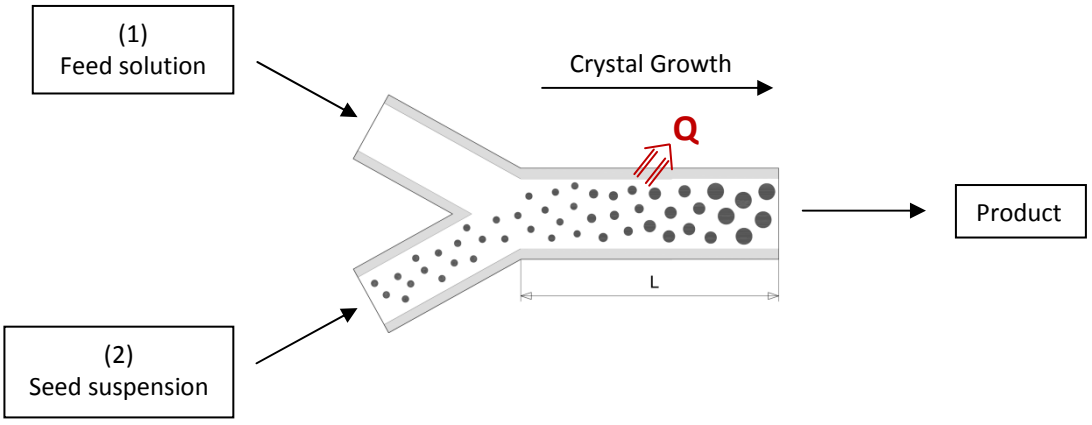

Figure 5: Schematic of the seeded tubular crystallizer

3.1. Influencing Parameters

As a first step to understand the crystallization process, the parameters that have an influence on the process had to be defined:

- chemicals (solubility, density)
- concentrations (supersaturation rate)
- flow rate (mixing behavior, shear stress)
- residence time
- seed load (particle interaction, nucleation)
- cooling rate and temperatures
- agglomeration and particle breakage

3.2. Experimental Schedule

Goals:

- Assay process parameters and design a robust process
- Control the crystallization process (nucleation and growth)
- Create optimal crystallization conditions (yield, specifications, reactor design)
- Find analysis methods (reliable, fast, cheap, reproducible)

In order to reach the above stated goals the reactor design should permit a series of variations:

- Variation of reactor length
- Variation of flow rate
- Variation of concentration/seed load
- Variation of temperature and cooling medium/rate

Two different series of experiments were projected to define the impact of single influencing parameters on the process. In the beginning, the ASA concentration of both the ASA-EtOH solution and the seeded ethanolic suspension was kept constant, as well as the flow ratio of both inlet flows. The influence of the residence time on the NMD and the CSD was investigated by varying both reactor length and total flow rate. In addition, different cooling media and cooling gradients were tested.

Experimental series:

- Exp S1 (a): Series with air cooling at room temperature, variation of reactor length and flow rate (see Table 1)
- Exp S1 (b): Series with intense cooling through multiple water cooling segments (see Table 2)
- Exp S2: Series with constant temperature (30°C) through a heated water bath, variation of reactor length and flow rate (see Table 3)

Table 1: Exp S1 (a) - experiments with air cooling

Reactor length	[m]	7	10	15	15	15
Flow rate	[ml/min]	11.4	11.4	11.4	17.4	23.4
Residence time	[s]	116	165	248	162	121
Cool. medium		air	air	air	air	air
Temperature	[°C]	r.T.	r.T.	r.T.	r.T.	r.T.

Table 2: Exp S1 (b) - experiments with water cooling

Reactor length	[m]	15					
Flow rate	[ml/min]	11.4					
Residence time	[s]	248					
Coil	no.	1	2	3	4	5	6
Length	[m]	2	2	2	1	1	1
cool. medium		air	air	water	water/ice	water/ice	ice
Temperature	[°C]	r.T.	r.T.	15	10	5	0

Table 3: Exp S2 - experiments with constant temperature

Reactor length	[m]	3	7	10	15	15	15
Flow rate	[ml/min]	11.4	11.4	11.4	11.4	15.3	22.4
Residence time	[s]	50	116	165	248	185	126
Cool. medium		water	water	water	water	water	water
Temperature	[°C]	30	30	30	30	30	30

4. Reactor Design

A novel crystallizer concept was developed that enabled to change the reactor conditions easily by altering reactor length and diameter, flow rate, and cooling conditions. Starting from the idea of the advantages of microstructured devices, considering optimized heat exchange conditions and process control, a tubular reactor was chosen. A reactor tube with an inner diameter of 2.0 mm was selected to allow larger crystal sizes, advantages regarding choking, and a higher throughput compared to microstructures. The tube consisted of synthetic material with good heat exchange qualities but also resistant to chemicals. The set-up was aimed to be simple and low-cost. Cooling was achieved by air convection and/or by implementing water baths. The use of water baths was convenient because the desired temperature could easily be adjusted and kept constant and the heat capacity of water guaranteed a fast heat transfer. As a first approach the seed suspension and feed solution were provided batch-wise.

To convey the fluid through the reactor, two peristaltic pumps were chosen. This avoided any direct contact of the solution with the pump. Otherwise, given the high volatility of EtOH, encrustations (fouling) could form inside the pumps during stop-periods, posing a problem to clean any enclosed device. Pumping tubes composed of material highly resistant to chemicals were used to avoid early decomposition.

4.1. First Reactor Concept

In preliminary tests a heated ASA-EtOH solution was pumped from a storage vessel through a polysiloxane tube. Primary nucleation occurred as the solution cooled down and got below the saturation limit. The amount of nuclei generated by cooling through air convection at room temperature was rather low. Cooling through water baths on the other hand resulted in strong primary nucleation. It proved to be difficult to run the crystallization process for a longer time period, because the high load of the suspension resulted easily in plugging of the tube.

As the preliminary tests had shown, crystallization where only primary nucleation occurred was difficult to control and in most cases led to plugging of the reactor tube. After considering literature discussing this topic [6],[18], the focus remained on the concept of introducing seed particles to suppress uncontrolled nucleation. The idea was to feed a seeded ASA-EtOH suspension to the reactor and mix it with a heated ASA-EtOH solution. Due to cooling supersaturation is created and the seed crystals grow. A first reactor concept of a continuously seeded tubular crystallizer was developed that consisted of a polysiloxane tube as main reactor part and two storage vessels, one for the feed solution and one for the seed suspension. The inlet flows were pumped with two peristaltic pumps from the repositories and mixed in a T-junction piece at the entrance of the reactor tube.

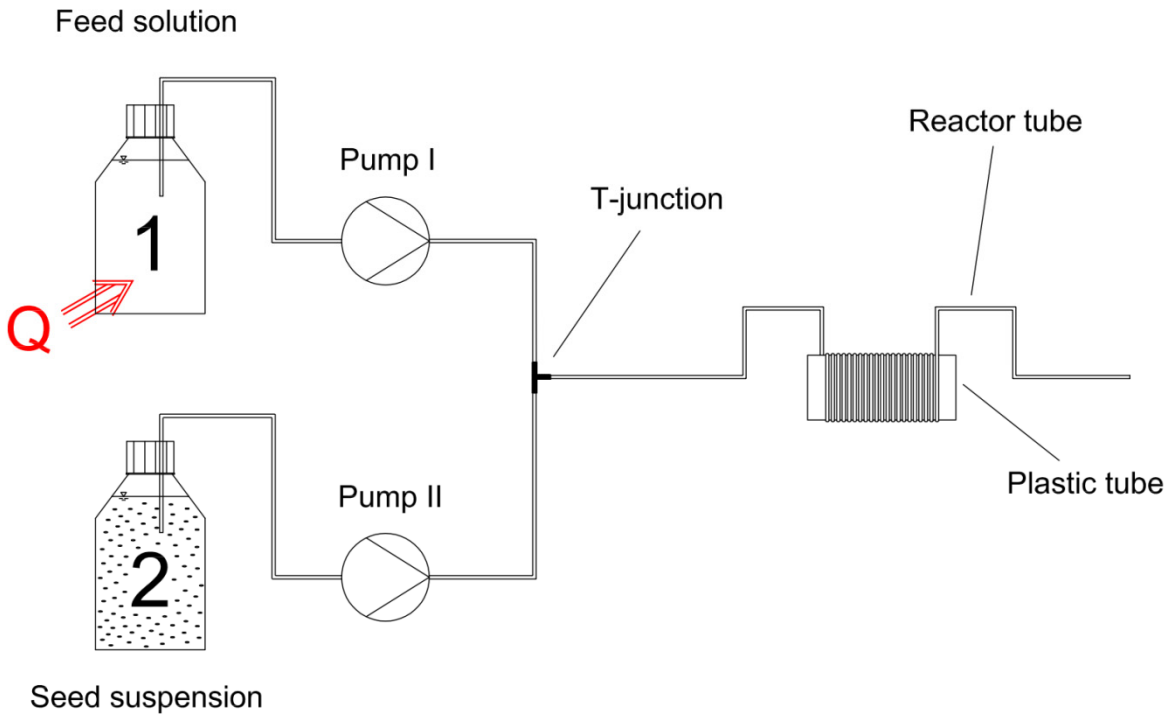

Figure 6: Reactor concept for mixing an ASA-EtOH solution with a seeded ethanolic suspension

Figure 6 shows the set-up of the first reactor concept. The reactor tube consisted of polysiloxane and had an inner diameter of 2.0 mm, an outer diameter of 4.0 mm, and a length of 16.5 m. It was coiled on several plastic tube piece with a diameter of 80 mm. An

Ismatec BVP-Process IP 65 – 3/6 peristaltic pump (pump I) was installed and equipped with PHARMED® tubing joined with polysiloxane connection tubes to convey the undersaturated ASA-EtOH-solution (1) to the reactor. An Ismatec Reglo Digital MS 2/6V 1.13C peristaltic pump (pump II), also equipped with PHARMED® tubing connected to polysiloxane junction tubes, was used to pump the seed suspension (2) from the storage vessel into the reactor tube. The storage vessel of solution 1 was placed in a heated water bath to maintain a constant temperature of 62°C and stirred with a blade stirrer. The temperature of the feed solution was appointed relatively high to allow a high supersaturation rate in order to increase the product yield. Suspension 2 was stored at room temperature and persistently stirred with a magnetic stirrer.

Junction pieces of different size and shape were tested for mixing the two inlet flows. In addition to a polypropylene (PP) T-piece, one consisting of glass was self crafted. The low surface roughness of glass was supposed to decrease encrustations during the mixing. Because of manufacturing limits, the glass component had a slightly larger diameter than the PP one, and was therefore dismissed to avoid a delay of the flow due to an enlargement of the cross. Great variations of the flow rates of the two inlet flows caused problems for T-shaped fittings by retarding the slower flow due to the pressure disproportion. Y-shaped fittings showed better mixing behavior, especially at lower flow rates. In the end a PP Y-fitting was chosen for further experimental runs. Tubes of the same material were used for all runs to assure steady conditions.

4.2. Reactor Concept with Air Cooling and Multiple Cooling Segments

A first experimental series Exp S1 was scheduled for testing varying reactor lengths and flow rates. The inner reactor diameter was left at 2.0 mm size and a reactor length of 15 m was chosen for the experimental tests with constant flow rates. In addition, two more reactor tubes with 7 and 10 m length were prepared for the tests with varying reactor length. The reactor tube was coiled around plastic tube pieces of 80 mm diameter each at different intervals. Each segment had a length of 1 or 2 m with 0.5 - 1 m spared space in between. The ASA-EtOH solution (1) was kept at 62 °C, while the seed suspension (2) was stored at room

temperature. The coils were stringed together and for Exp S1 (a) only cooled through air convection at room temperature that averaged 21.5 (± 0.5) °C. Figure 7 shows the reactor design for an exemplary reactor tube with 7m length that was coiled on two plastic tube pieces. Q stands for the heat applied or removed.

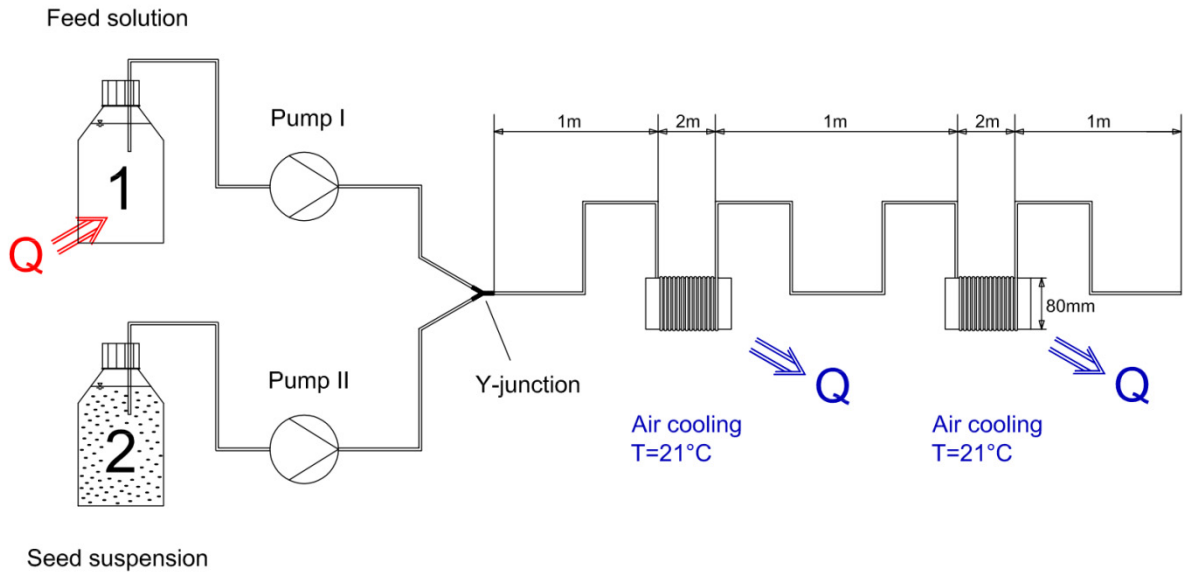

Figure 7: Reactor concept with air cooling for experimental series Exp S1 (a) (varying lengths)

More cooling sections were implemented for experimental series Exp S1 (b) to allow a multiple-stage cooling progression. For this purpose additional water baths were incorporated in the set-up and were kept at different temperatures by adding various amounts of ice to each. A step-wise cooling progression was aimed at to provide an increased supersaturation level throughout the whole reactor. The reactor set-up is shown in Figure 8.

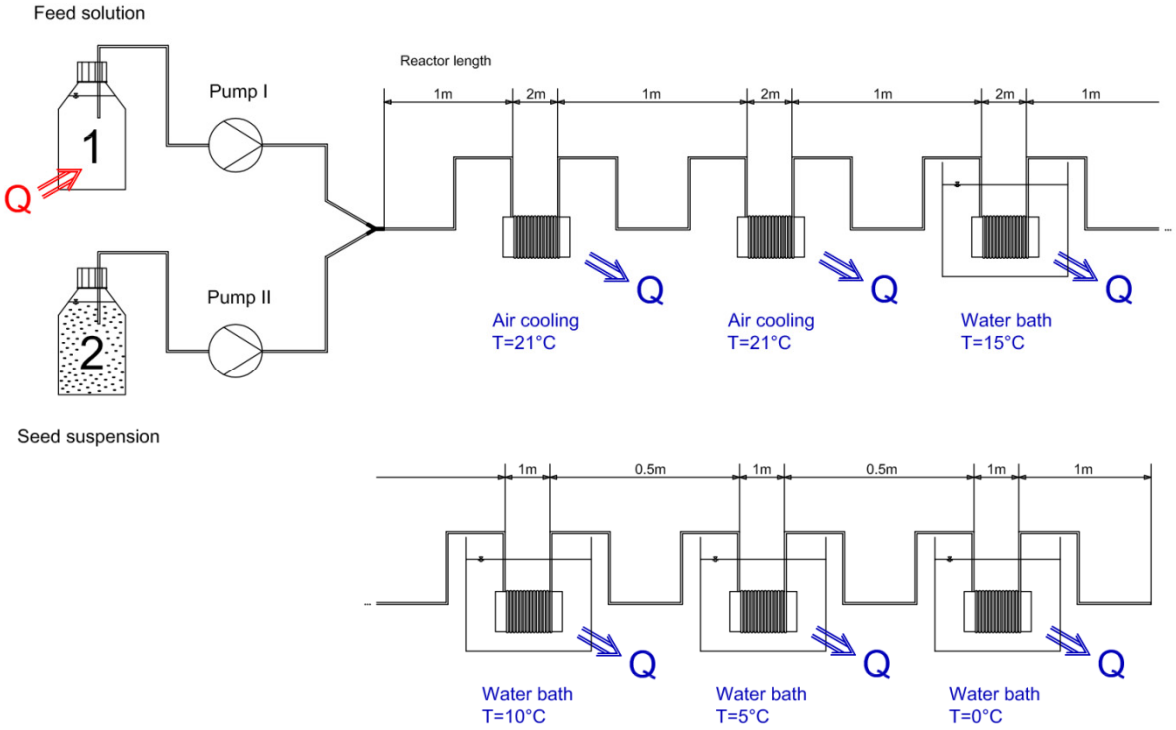

Figure 8: Reactor concept with multiple cooling segments for experimental series Exp S1 (b) (15m length)

4.3. Reactor Concept with Constant Temperature

Experimental Series Exp S2 was designed to investigate the influence of varying reactor lengths and flow rates on the crystallization behavior while keeping the reactor temperature constant. The general idea was to exclude the influence of a changing saturation limit due to varying temperature. Reactor tube lengths of 3 m, 7 m, 10 m, and 15 m were applied. The reactor tube was no longer coiled around a synthetic tube, but coiled around a bended 0.1 m diameter metal frame to improve the heat transfer in the water bath, compared to the plastic tubes used in prior runs. To additionally increase the heat transfer, a circular flow was established inside the water bath. For this purpose a synthetic tube was connected to an external centrifugal pump and placed on each side of the water bath in a way to create cross flow. The whole reactor was placed into the water bath. Only an initial part of 1 m length was spared for the practicability of joining the different set-up components, and also a 0.4 m

piece of tube at the end of the reactor to take samples and to apply ultrasonic irradiation to study the effect on the product crystals. A single water bath was installed to maintain a constant external temperature. The temperature was appointed 30°C, and therefore somewhat below the temperature of the solution measured right after the mixing piece (37 ±3 °C). The reactor segment of 1 m length leading from the Y-fitting to the tempered section resulted in a further temperature decrease of the suspension due to air convection at room temperature (25 ±1.5 °C). The reactor set-up for different lengths is shown in Figure 9.

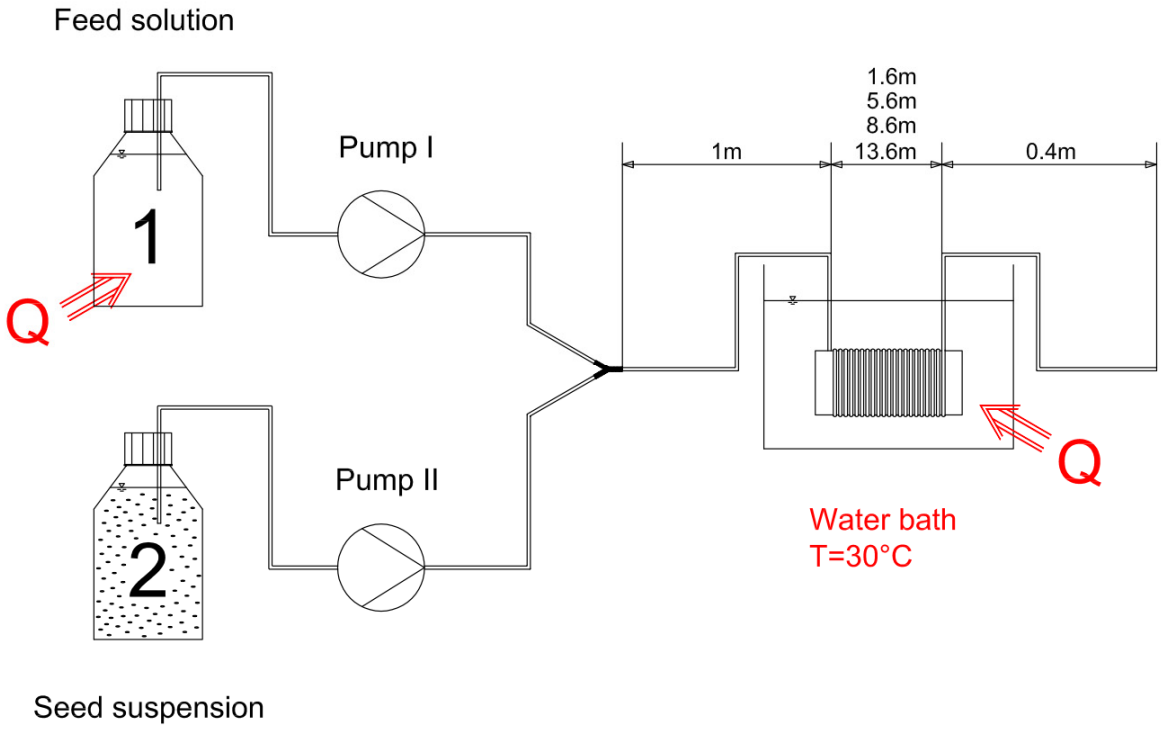

Figure 9: Reactor concept with constant temperature for experimental series Exp S2 (varying lengths)

5. Experimental Procedure

5.1. Preparations for an Experimental Run

In order to perform a successful experimental run, some preliminary preparations had to be done before each test. This included the assembling of the equipment, the calibration of the pumps and the preparation of the sampling equipment.

5.1.1. Pump Calibration

Both peristaltic pumps were calibrated before every new series of runs. This was done to avoid deviations from run to run, because the peristaltic pumps were dissembled after completing each test run to avoid damages on the tubes.

5.1.2. Preparation of Feed Solution (1)

The feed solution was prepared in order to bring a slightly undersaturated ASA-EtOH mixture at an elevated temperature into the reactor. The same ASA-EtOH ratio was used for all runs to ensure full comparability and was appointed to 50g ASA per 100g EtOH. It was brought to a constant temperature of 60°C and stirred for at least 30 minutes with a blade agitator before the run was started. At this temperature the ASA was completely dissolved and the solution still undersaturated.

5.1.3. Preparation of Seed Suspension (2)

An ASA-EtOH suspension was prepared in order to feed seed particles into the reactor, and therefore referred to as seed suspension. 50g ASA per 100g ethanol were stirred at room temperature for at least 48 hours to ensure thermodynamic equilibrium of the solid and liquid phase. The amount of ASA exceeded the saturation limit of the solution so that undissolved crystalline ASA formed seed crystals. A magnetic stirrer was used to create a

homogenous suspension. The temperature of the solution averaged 2°C higher then room temperature because of heat dissipation due to the mixing.

5.1.4. Preparation of the Equipment

All fittings were checked to avoid bursting during the run. The different cooling sections were brought to the required temperatures by adding ice into the water baths, and kept constant by repeating this in certain intervals according to the temperature. The temperature of both storage vessels and the temperature at the mixing point and the reactor end was measured. To measure the temperature at the mixing point, the reactor tube was disconnected from the mixing segment and measurements were performed directly in the Y-fitting. All equipment needed for sample taking was prepared. The filter pump was installed and all beakers, filters, and frits were weighed out and labeled.

5.2. Experimental Run

5.2.1. Start-up Procedure

After completing all preparations explained before, the start-up process could be initialized. Before each run, the reactor tube was rinsed with warm ethanol to detach eventual incrustations from previous runs and to preheat the tube. For this purpose pump I was used and afterwards was switched back to feed solution 1. It proved to be necessary to feed the seed suspension into the reactor first before adding solution 1 to the system. Otherwise strong nucleation would take place due to supersaturation caused by decreasing temperature along the reactor, and the tube would plug.

5.2.2. Sampling

A sample of the seed suspension was taken directly from the suspension vessel to have an impression of the current CSD of the seeds. After the process reached steady state and was stable, the first product sample was taken at the reactor outlet. Two more were taken at regular intervals. Before the last sample ultrasonic irradiation was applied at a small segment at the end of the reactor to investigate what effect this would have on the product. The samples were taken by pouring the outflow over a suction filter. A fast separation of the solid and liquid phase was necessary to prevent further growing of the crystals as the ethanol evaporated. To successfully separate the solids from the solution the filter cake was washed with cyclohexan. The sample was then dried in a drying furnace. In a first attempt, filter paper was used to collect the crystallized ASA. The filter paper was weighted beforehand and afterwards. Subsequently, suction strainers were used whose mass difference was assessed. To double-check the mass balance, the mass and the concentration of the liquid phase in the collecting vessel was measured.

5.3. Troubleshooting

5.3.1. Reactor Plugging

Absence or a too small amount of seeds resulted in strong primary nucleation and consequently plugging of the tube. Tube plugging also occurred if the flow rates were too low. Different flow rates of the two feed flows caused problems at the Y-fitting. At very low flow rates a pulsing (because of the peristaltic pump), non-steady mixing behavior was observed. Retarded and even reverse flow if one pump was inactive lead to uncontrolled primary nucleation and as a consequence to blockage of the reactor. To free the reactor tube after plugging, it was rinsed with warm EtOH and placed in a warm water bath. Also mechanical treatment and ultrasonic vibration were applied to lose the incrustations formed in the tube.

5.3.2. Varying Seed Feed Rate

An evaluation of the seed feed samples of all test runs showed, that the NMD varied in a scale of ± 10 µm. The variation of seeds probably occurred due to batch-wise production of the seed suspension, because different charges were not always of the same age and temperature, as well as the agitator speed of the magnetic stirrer varied slightly.

A test run regarding the constancy of the seed amount fed to the mixing zone over a certain time period showed a variation up to 7 % mass of seeds. However, statistical fluctuations have to be considered, and this variation is still within the common range.

5.3.3. Varying Operating Conditions

Given the fact that the process was run only semi-continuously it could happen that the feed solution run out during an experiment that took longer. This occurred when a run had to be restarted because of early plugging, the flow rate was high, or a longer run was scheduled. The room temperature varied in different experimental series because they were carried out during different seasons. A variation of the room temperature was also observed during some runs if they took longer and due to external influences.

5.3.4. Sampling

Because of the high volatility of EtOH, additional crystallization and coalescence of particles occurred during the sampling. The use of cylcohexan prevented further crystal growth but eliminated the possibility to counter check the concentration and total mass of the liquid phase. Difficulties regarding the assessing of absolute masses were come across by using both filters and suction strainers, because the suction output through the filter was rather low and a layer of ASA remained on the side of the suction strainer. At very low flow rates an error in measuring the absolute masses could happen because the mass output at the end of the reactor occurred only droplet-wise.

5.3.5. Measurement of Temperatures

No inline/online measurements were performed because the available sensors were not designed for this purpose. In order to measure the temperature inside the small reactor tube, a PT 100 thermocouple element was used. Despite the small diameter of 1.0 mm it inevitably hindered the flow of particles because it had to be inserted against flow direction. Because of the high volatility of EtOH and the cooling effect associated with evaporation of liquids, the temperature assessed could show a variation of 2-4 degree Celsius, depending on the sensor position inside the tube.

5.4. Special Fields of Interest

5.4.1. Seed Production

In an ideal case all seed particles should have the exact same size and shape. Actual manufacturing aims to keep the particle size distribution as narrow as possible and always in the same range to obtain constant product properties and quality.

Different methods of generating seed particles were tested to find the one most suited for application in the crystallization process. The influence of different stirring methods, precipitation through supersaturation due to cooling, and particle classification methods were assayed.

1.) In a first approach seed particles were selected by sieving a certain fraction of commercially available ASA. This method was discarded because of a series of problems. The elongate shape of the particles turned out to be unfavorable for the sieving process and the electrostatic charge during the process lead to blockage of the screens. Using a sieve-tower resulted in heavy dust generation. Preserving the desired CSD and shape of the particles when bringing a crystal size fraction into a saturated solution also proved to be difficult because of solution and dissolution procedures and friction effects.

2.) Milling ASA particles with a ball mill was tested. The result was a large amount of fines with some large particles. To exclude the possibility of still integer particles rather long milling periods would be required. During the milling process an odor of acetic acid was noticed. The milling most likely caused hot spots that favored a decomposition of the ASA. The result of this test confirmed observations noted in other publications [4].

3.) Particles were created from solution by precipitation through cooling. Commercially available ASA was dissolved in EtOH at 62°C. The solution was then cooled down rapidly in an ice bath and crystals formed as the supersaturation limit was reached. This method worked well but was not pursued in future tests.

4.) The method of choice was to generate a supersaturated suspension by mixing commercially available ASA with EtOH in a ratio that exceeded the solubility limit. The suspension was mixed with a magnetic stirrer for at least 48 hours to ensure thermodynamic equilibrium of the solid and liquid phase at room temperature. The ASA/EtOH ratio and the

temperature were kept constant to ensure steady seed load. This method was chosen in the end because of the low effort required and the high reproducibility.

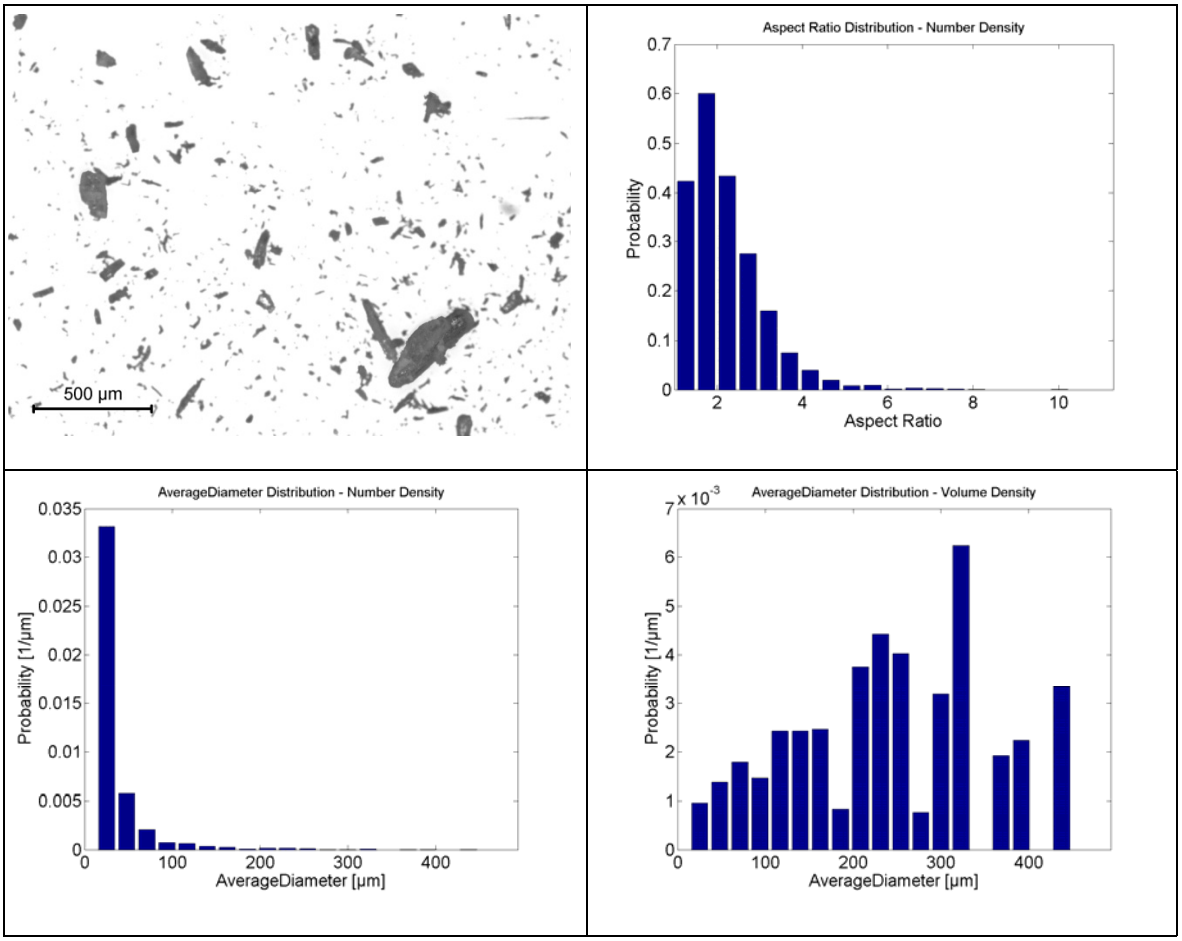

Figure 10: Top left-hand: ASA crystals treated with a ball mill. Top right-hand: Aspect ratio number density. Bottom left-hand: Average diameter number density. Bottom right-hand: Average diameter volume density

ad 1.) Figure 10 shows ASA crystals after they were milled with a ball mill with 19 balls of 10 mm diameter each for 10 min. This procedure produced a large amount of very small fines while it let some larger particles integer. Longer milling times would reduce the fraction of large particles but also produce more fines. The very large CSD however is unfavorable and so is the resulting average volume mean diameter.

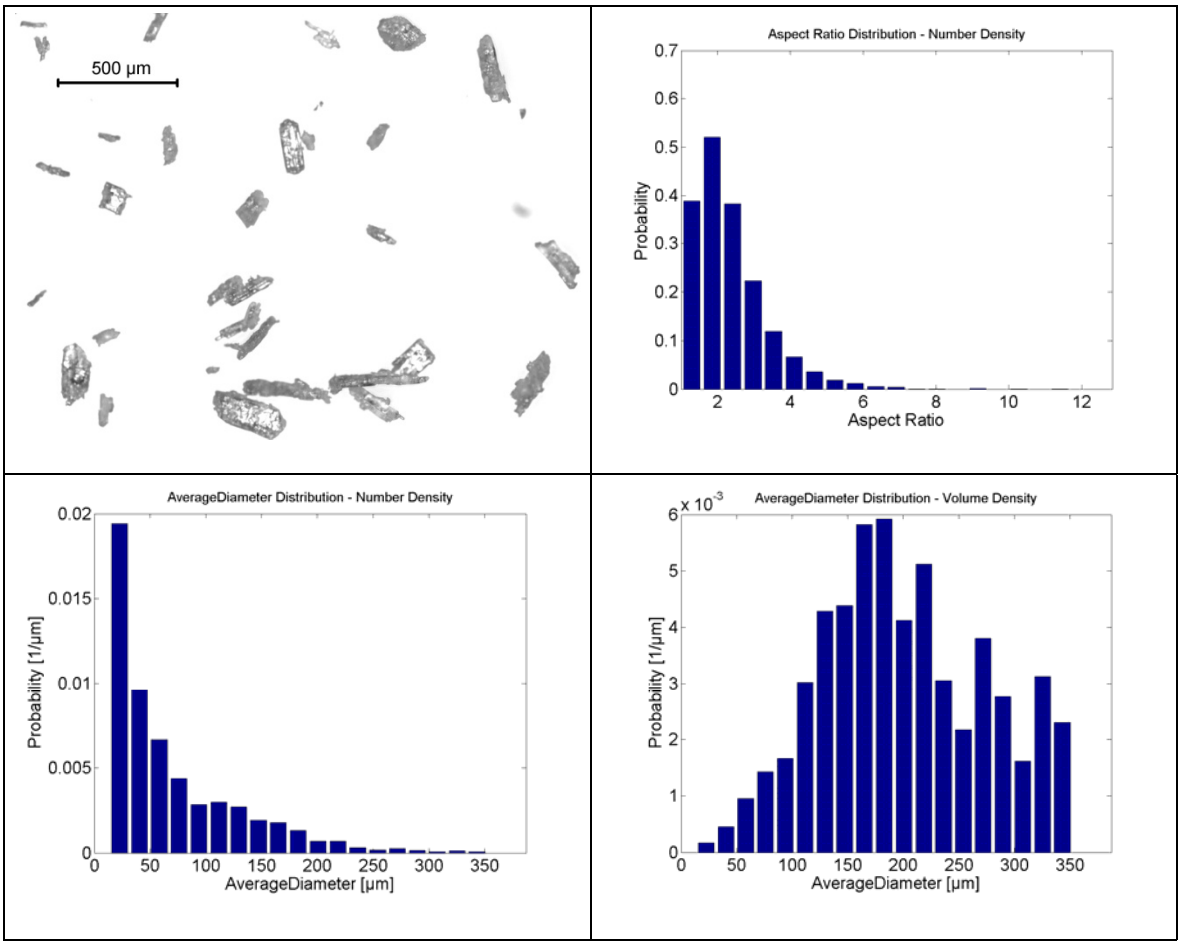

Figure 11: Top left-hand: ASA crystals generated with a ball mill after being suspended in an ASA-EtOH solution. Top right-hand: Aspect ratio number density. Bottom left-hand: Average diameter number density. Bottom right-hand: Average diameter volume density

ad 2.) The milled ASA crystals were added to a saturated ASA-EtOH-solution at room temperature and stirred for 48 hours. Samples were taken at different intervals to check if the consistency of the newly added crystals changed over time. No significant changes were observed. Figure 11 shows an exemplary sample. The amount of very small particles was diminished compared to the input distribution in Figure 10. Although the solution was considered saturated, solution and dissolution procedures may have occurred as described in literature [18], causing very small particles to vanish and others to grow (Ostwald ripening, see chap. 2.3.3). However, the CSD continued to give a disadvantageous seed input because of the very broad range.

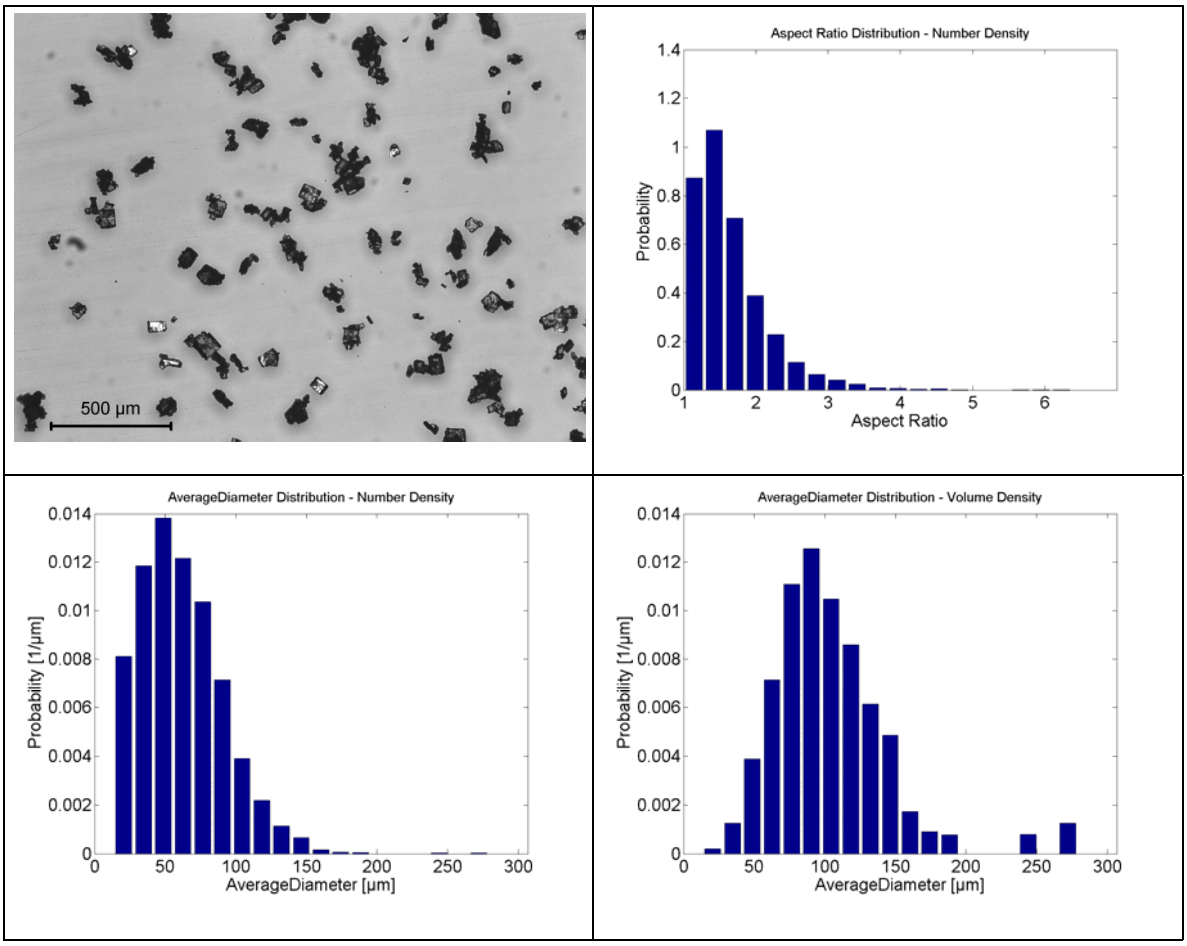

Figure 12: Top left-hand: ASA crystals generated through precipitation. Top right-hand: Aspect ratio number density. Bottom left-hand: Average diameter number density. Bottom right-hand: Average diameter volume density

ad 3) Figure 12 shows ASA crystals produced through precipitation from a heated solution through intense cooling in an ice bath. The suspension was mixed during the procedure and ultrasonic vibration was applied to get a better dispersion. The mean diameter and narrow CSD in the range of 20-200 µm was a very promising. However, method 4 was chosen to create seed particles as it required less effort and produced favorable and reproducible results likewise.

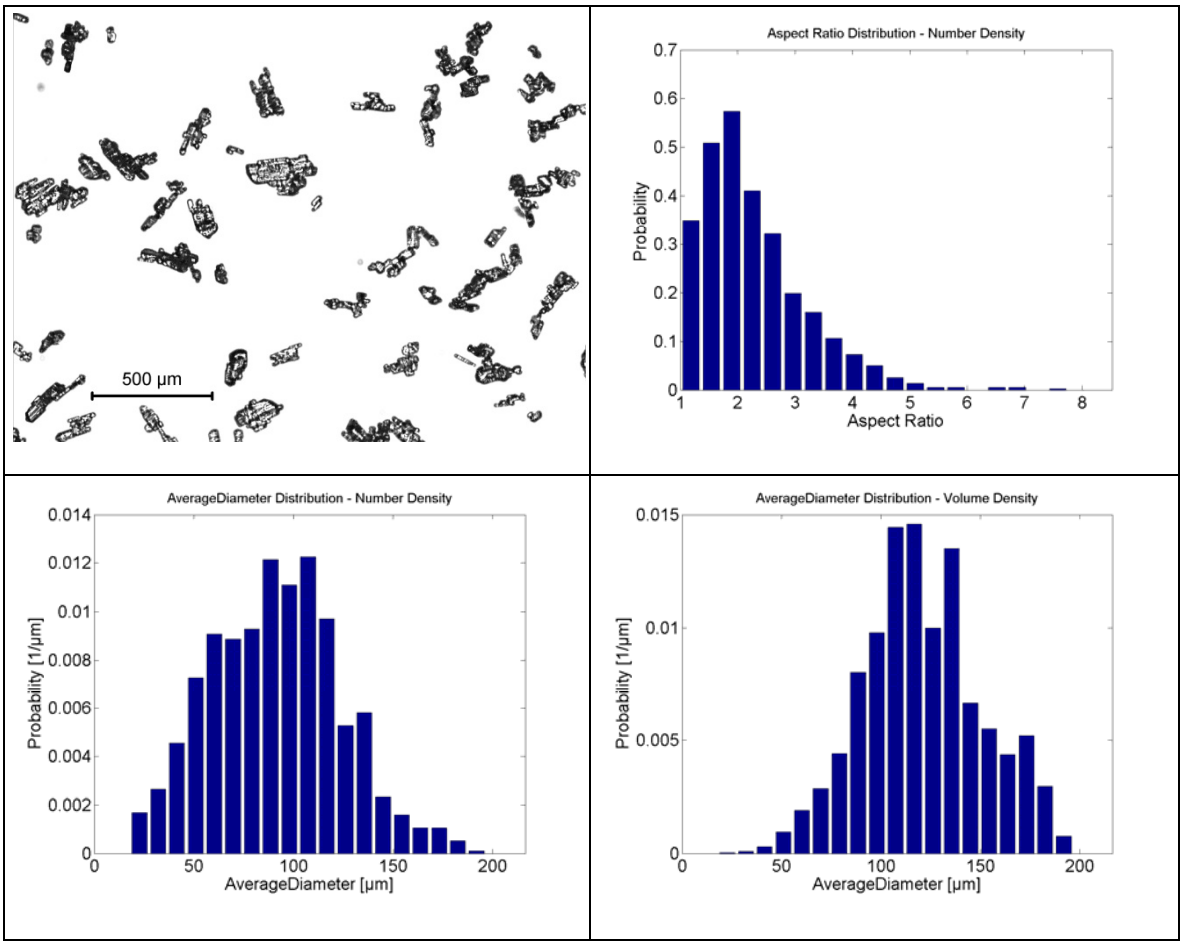

Figure 13: Top left-hand: ASA particles produced of solution at room temperature. Top right-hand: Aspect ratio number density. Bottom left-hand: Average diameter number density. Bottom right-hand: Average diameter volume density

ad 4) Seed crystals generated from a suspension at room temperature are shown in Figure 13. An excess of ASA was added to an EtOH-solution and stirred for 48 hours with a magnetic stirrer. This method produced seed crystals with a constant CSD of approximately 50-200 µm. The use of a different stirrer would probably enable to achieve a narrower CSD. The magnetic stirrer in use offered rather limited possibilities to control the mixing properties inside the storage vessel, and also produced additional fines by destroying the particles in the bottom area.

All methods presented so far aim at batch-wise production. To accomplish a continuously operated crystallization process, seed particles must be generated and fed into the reactor in a continuously way as well. The batch-wise generation of seeds was chosen in order to gain operating experience with the crystallizer as a first step, and implementing a continuous seed generation step once the actual crystallization process was understood and controlled.

The best method to generate seed particles would be to produce them in the process. This could be done by classifying the product flow and recycling the fine fraction. Due to the rather low amount of fines present in the product flow, an additional operating step (e.g. ultrasonic irradiation, milling) to reduce the particle size of the recycled fraction could be necessary for sufficient seed input. Classification devices like fine traps are already applied in continuously operated industrial crystallizers. The most common procedures are elutriation in gravity vessels or the use of hydrocyclones [18]. Figure 14 shows a schematic of a possible recycle flow with fines classification and ultrasonic irradiation applied to decrease the seed particle size.

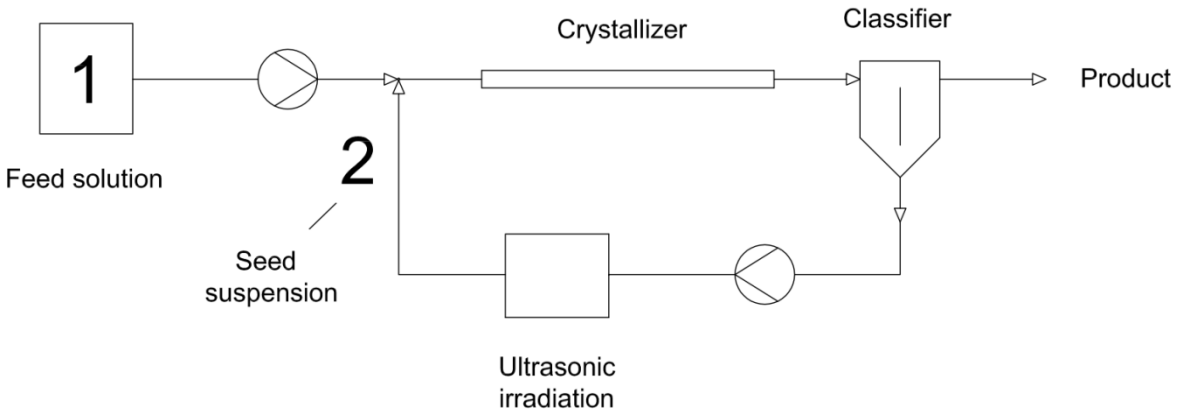

Figure 14: Flow chart of a continuous process with fine particles recycling

5.4.2. Application of Ultrasonic Irradiation

Various authors already investigated the influence of ultrasonic irradiation on the crystal size and size distribution. The findings are that agglomeration and the resulting crystal size were clearly reduced by applying ultrasonic vibrations [3]. Incrustations in crystallizers can also be reduced or even avoided in some cases, but it is still problematic to maintain these operating conditions for a longer period. Scale-up of vibrators for larger crystallization apparatuses is also problematic [18]. A study [21] that investigated the effect of ultrasonic irradiation on the number of ASA crystals produced showed, that there is a certain energy input required to activate primary nucleation. Low supersaturation and only short irradiation time resulted in a decrease of primary nucleation. Longer irradiation time led to an increase of primary nucleation.

The application of ultrasonic vibration was introduced to the system to study the effects that such a treatment would have on the product. At the end of each run the rear section of the reactor tube (30 cm length) was exposed to ultrasonic vibration. This was done for several minutes and a sample was taken subsequently.

Ultrasonic irradiation had a strong effect on the NMD. The average NMD was clearly smaller than the product NMD without this treatment. This lead to the conclusion, that agglomerates were destroyed, but possibly also some larger particles because the product particles already proved to be fragile in other particle analysis attempts. An optical analysis of the samples showed that the shape of the crystals did not differ significantly from product crystals without ultrasonic irradiation treatment. Figure 15 and Figure 16 show an optical evaluation of seed crystals and product crystals with and without ultrasonic irradiation applied from two exemplarily runs.

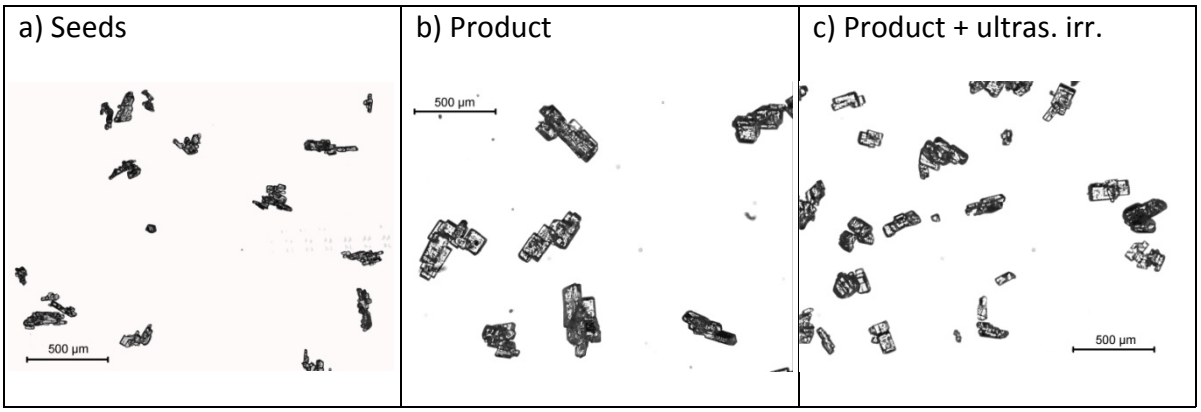

Figure 15: Optical evaluation of crystals (Volume flow = 8.9 (P I) + 2.5 (PII) ml/min, 7m reactor length).
a) Seed sample b) product sample without ultrasonic irradiation c) product sample with ultrasonic irradiation

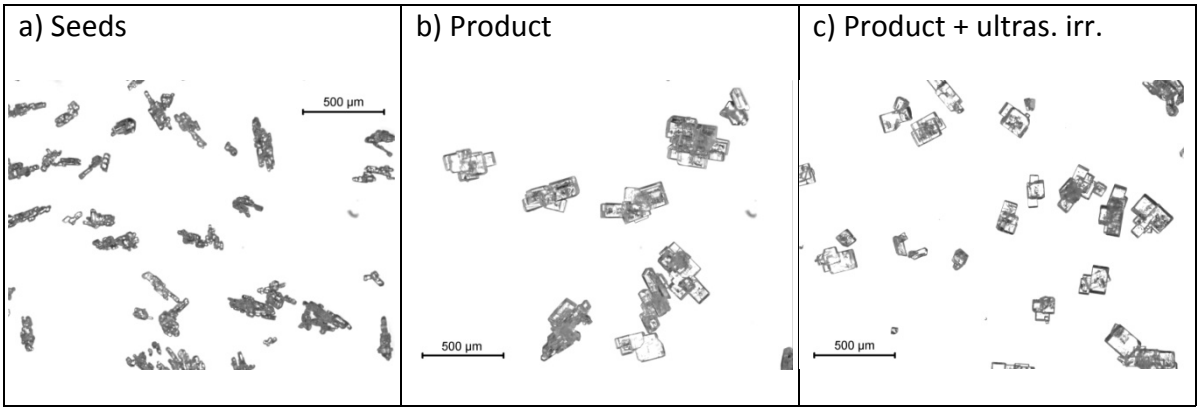

Figure 16: Optical evaluation of crystals (Volume flow = 12 (P I) + 3.3 (PII) ml/min, 15m reactor length)
a) Seed sample b) product sample without ultrasonic irradiation c) product sample with ultrasonic irradiation

Figure 17 shows a sample evaluation with a Malvern Morphologi G3 particle characterization device. The seed sample and product samples 2 and 3 did not undergo ultrasonic irradiation. The CSD of sample 2 and 3 only showed a slight deviation from each other (probably because of statistical fluctuation), but were clearly distinguishable from the seed CSD. Sample 4 had been treated with ultrasonic irradiation and showed a clearly diminished average volume diameter compared to sample 2 and 3 and therefore verified the microscope analysis.

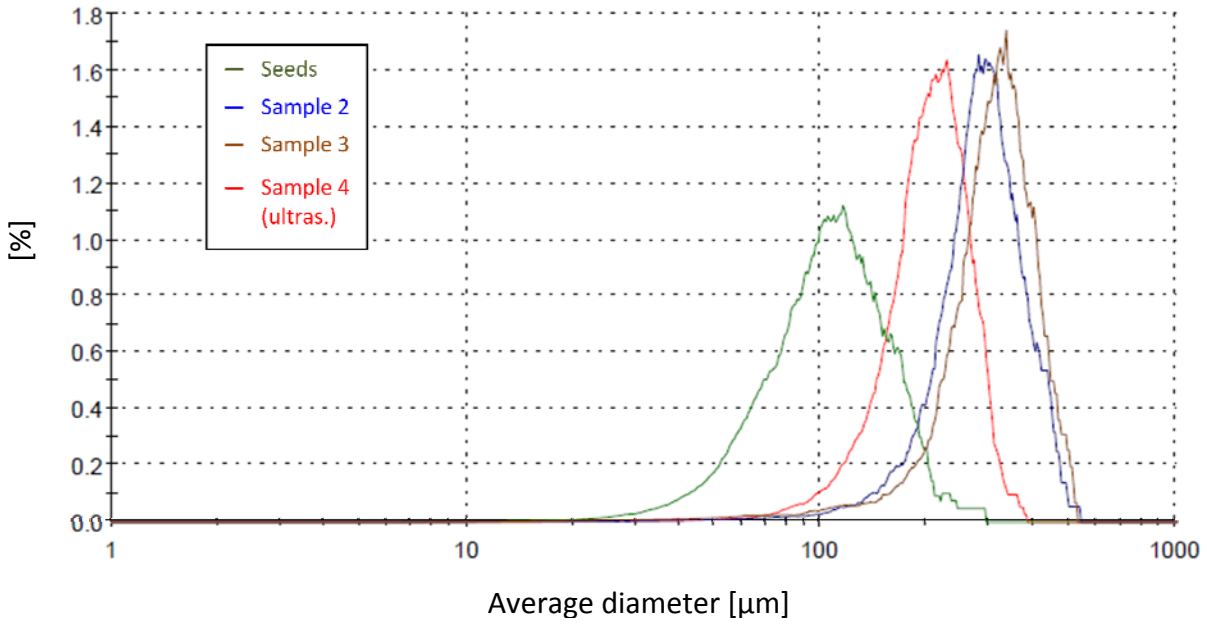

Figure 17: Average volume diameter distribution of seed and product samples without and with ultrasonic irradiation analyzed with Malvern Morphologi G3

6. Evaluation of Experimental Data

6.1. Image Analysis

An optical analysis of the seed and product particles was performed. For this purpose samples were taken from each run. A reflected-light microscope Laica DM 4000 with a Laica DFC 290 digital camera attachment was used for the evaluation. Per sample 150-200 pictures were taken showing approximately 800-1000 particles, allowing a representative evaluation [22]. The pictures were processed with the open source software program ImageJ v. 1.42q that provided the data for the statistical evaluation.

6.1.1. Image Evaluation Procedure with ImageJ

ImageJ is a public domain open source software. It can display, edit, analyze, and process images. It is possible to calculate area and pixel value statistics and create density histograms and line profile plots [23]. In our case the software not only counted the particles, it also gave information about the particle perimeter, the area, the maximum and minimum axes, the feret diameter, and the aspect ratio.

Figure 18 gives a short overview of the image evaluation procedure with ImageJ. The images were loaded into the program and converted to 8-bit grayscale (step 1). The scale was reset to zero and the desired output parameters were defined (step 2). A threshold value was defined to segment the image into features of interest and background (step 3). The processing settings to exclude particles on edges, draw outlines and create a result file were selected and the image analysis was performed (step 4). After the image analysis the resulting particle count (see Figure 19) was manually checked for unwanted counts, like agglomerates.

Step 1:

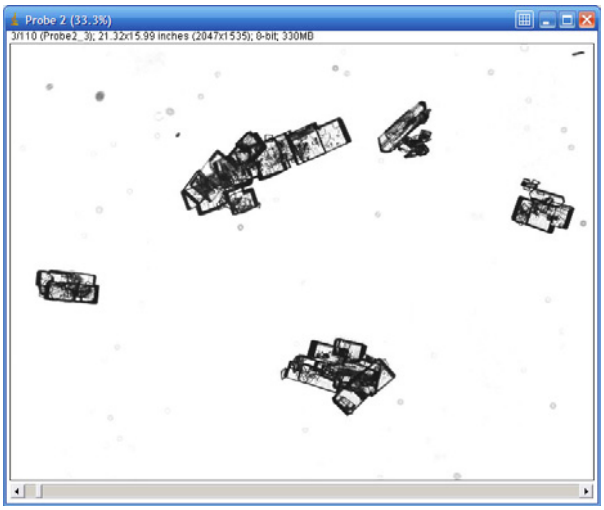

Step 2:

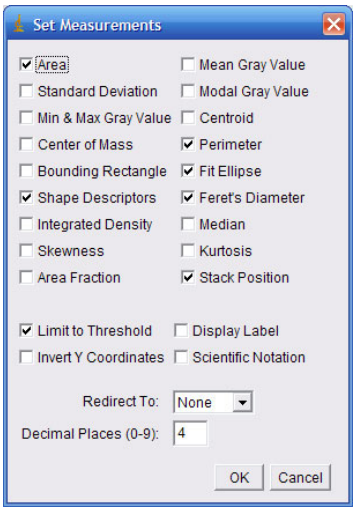

Step 3:

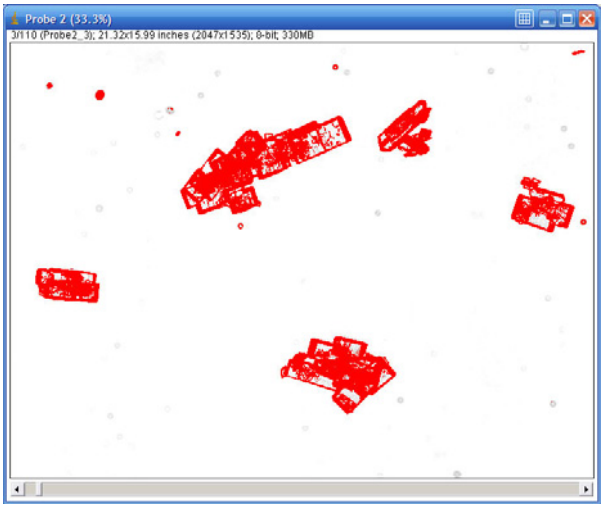

Step 4:

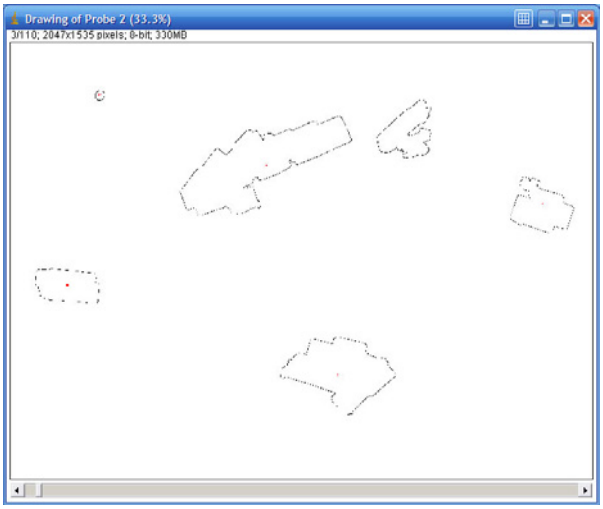

Figure 18: Evaluation procedure with ImageJ

Results

File Edit Font

	Area	Perim.	Major	Minor	Angle	Circ.	Feret	Slice	FeretAngle	MinFeret	AR	Round	Solidity
1	53198	1202.9302	374.5188	180.8556	45.9938	0.4620	373.1729	1	66.8014	206.5374	2.0708	0.4829	0.8514
2	1485	189.3797	53.8280	35.1260	27.4457	0.5203	57.2014	1	36.4692	36.6300	1.5324	0.6526	0.8621
3	9379	421.8549	146.8376	81.3260	40.7711	0.6623	149.8833	1	28.2749	77.7599	1.8055	0.5538	0.9265
4	2074	189.2548	55.0530	47.9665	135.4855	0.7277	65.2993	1	130.0303	47	1.1477	0.8713	0.9257
5	1269	173.4802	63.8582	25.3020	149.4241	0.5299	64.4981	1	150.2551	29.6578	2.5238	0.3962	0.8073
6	15956	577.9899	144.9778	140.1305	105.5353	0.6002	163.2176	1	126.0274	140.5248	1.0346	0.9666	0.9075
7	55361	1281.0378	451.8250	156.0069	127.5536	0.4239	437.4711	2	124.8525	197.7361	2.8962	0.3453	0.8045
8	101665	2054.7750	420.8938	307.5453	62.2395	0.3026	474.5240	2	62.7870	331.8611	1.3686	0.7307	0.8632
9	59851	1725.5719	366.5789	207.8806	32.0923	0.2526	401.3191	2	24.9048	239.4128	1.7634	0.5671	0.8424
10	60386	1398.2813	488.7850	157.2999	4.6919	0.3881	483.9225	2	16.0755	196.7679	3.1073	0.3218	0.8465
11	14667	658.8011	182.8860	102.1106	164.1665	0.4247	205.6648	2	170.7667	117.6855	1.7911	0.5583	0.8451
12	353	100.1838	46.6759	9.6292	10.2201	0.4420	44.7214	3	10.3048	10.7734	4.8473	0.2063	0.8770
13	476	81.8406	26.0304	23.2828	65.6750	0.8931	27.2029	3	72.8973	23.7524	1.1180	0.8944	0.9454
14	21952	974.7981	193.0898	144.7521	47.7537	0.2903	235.8495	3	48.2656	161.8136	1.3339	0.7497	0.8218

Figure 19: Results table generated by ImageJ

6.1.2. Verification of the Sample Analysis

In order to verify the sample evaluation method done with the microscope, test measurements with a Malvern Morphologi G3 particle characterization device were performed. The results gained with this evaluation method confirmed the results from the evaluation method chosen in the first place.

Figure 20 shows an exemplary study of selected particles. The particles did not show any deviations in size and shape compared to the ones analyzed with the microscope so it was assumed that sub-sampling was done accurately and no particles were destroyed during that process.

Figure 20: Study of size and shape of selected particles

6.2. Particle Characteristics

In an ideal case all particles would have the exact same size and shape. In a technical crystallization process however, crystals can differ significantly in size and shape.

6.2.1. Shape Factors

Crystals can have a large variety of shapes, like cubic, spherical, needle-like, platelets etc. [24]. Shape factors are used to describe and compare particles with unequal profiles.

The aspect ratio AR is a function of the largest diameter d_{max} and the smallest diameter d_{min} orthogonal to it.

$$AR = \frac{d_{min}}{d_{max}} \tag{6.1}$$

Another shape factor is the circularity (sphericity) of Wadell ψ that is defined as the ratio of the equivalent volume diameter x_v to the equivalent surface diameter x_s and describes the deviation from a spherical shape. A value of 1.0 would indicate a perfect circle [22].

$$\Psi = \left(\frac{x_v}{x_s}\right)^2 \tag{6.2}$$

6.2.2. Equivalent Diameter

To indicate the size of a crystal a characteristic length is defined. The equivalent diameter of a sphere with the same physical properties as the particle is a fictional dimension that facilitates the comparison of different shaped particles. It can refer to different quantities like the equivalent surface area, the equivalent volume or equivalent mass.

The feret diameter is the distance between two parallel tangents on opposite sides of the particle.

6.2.3. Average Diameter

The average particle diameter d_p is calculated referring to the particle area A (in our case calculated by ImageJ) and is the diameter of a corresponding circle.

$$d_p = \frac{4A}{\pi} \tag{6.3}$$

6.2.4. Particle Volume

The particle volume V_x is calculated using the average diameter d_p and refers to a corresponding sphere.

$$V_x = \frac{d_p^3 \pi}{6} \tag{6.4}$$

6.2.5. Number Mean Diameter

The arithmetic number mean diameter (NMD) $\overline{d_p}$ is the mean value of the average diameter of n particles of one sample.

$$\overline{d_p} = \frac{1}{n} \sum_{i=1}^{n} d_{p,i} \tag{6.5}$$

6.2.6. Standard Deviation of the NMD

The deviation of the single diameters to the NMD is considered by calculating the standard deviation s. The number of diameters considered is n.

$$s = \sqrt{\frac{1}{n-1} \sum_{i=1}^{n} \left(d_{p,i} - \overline{d_p}\right)^2} \tag{6.6}$$

6.3. Particle Size Distribution

The particle size distribution (PSD) gives information about the relative amounts of particles present, sorted by size. For this purpose a certain amount of particle size classes with a related class range is defined.

6.3.1. Frequency (Density) Distribution

A typical statistical distribution is the Gauss error distribution or normal probability distribution $q_r(x)$ that indicates the relative frequency of the particles $\Delta Q_r(x)$ related to the class range Δx. The dimension r describes the aspect assigned to the distribution (r=0 number, r=1 length, r=2 surface area, r=3 volume).

$$\Delta Q_r(x) = \frac{\Delta m(x)}{m_{total}} \tag{6.7}$$

$$\Delta x = d_{p,o} - d_{p,u} \tag{6.8}$$

$$q_r(x) = \frac{\Delta Q_r}{\Delta x} \tag{6.9}$$

6.3.2. Cumulative Frequency

The cumulative frequency $Q_r(x)$ represents the percentage of all particles accumulated up to the particle diameter d_p. The sum of all particles up to $d_{p,max}$ is 1 (100%). Figure 21 shows a graphical representation of $q_r(x)$ and $Q_r(x)$.

$$Q_r\left(d_{p,max}\right) = \int_0^{d_{p,max}} q_r\,(x)dx = 1 \tag{6.10}$$

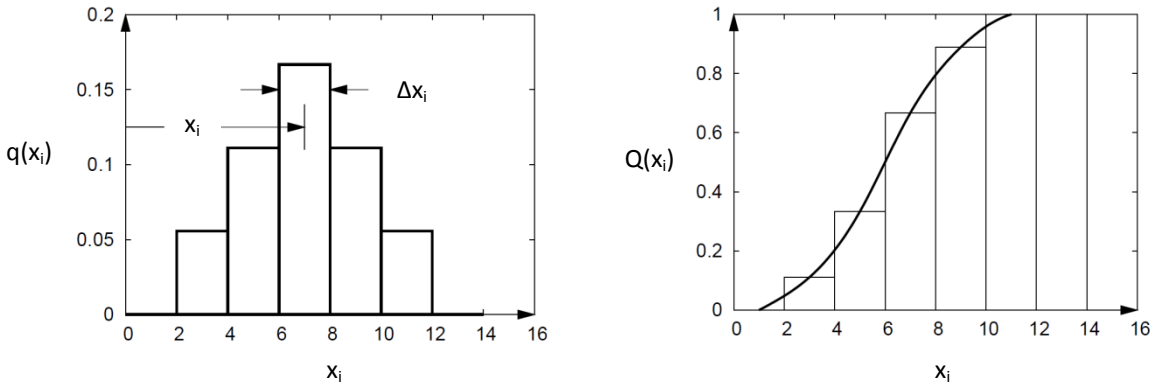

Figure 21: Left-hand: frequency (density) distribution q(x). Right-hand: cumulative distribution Q(x) (adapted from[25])

6.3.3. Logarithmic Normal Value Distribution

The particle size distribution can be approximated by a two parameter distribution. The first parameter is a characteristic value that characterizes the position on the x-axis, the second parameter describes the amplitude of the function. The logarithmic normal distribution (log NV) function uses the median diameter $d_{p,50}$ and the standard deviation σ as characteristic parameters. In general, the log-NV is used to describe particle distributions with high fines content.

$$q_3(d_p) = \frac{1}{\sigma d_p \sqrt{2\pi}} exp\left[-\frac{1}{2}\left(\frac{ln\left(\frac{d_p}{d_{p,50}}\right)}{\sigma}\right)^2\right] \tag{6.11}$$

The median diameter $d_{p,50}$ divides the area under the frequency curve into equal parts. All particles accumulated up to the volume diameter $d_{p,50}$ represent 50% of the total volume of all particles. The standard deviation σ shows the deviation of the single diameters compared to the median diameter.

$$\sigma = ln\left(\frac{d_{p,84}}{d_{p,50}}\right) = ln\left(\frac{d_{p,50}}{d_{p,16}}\right) \tag{6.12}$$

6.3.4. Results Particle Size Distribution and Number Mean Diameter

To compare different samples and test runs, a frequency distribution of the average diameter distribution and the aspect ratio considering number density, area density, and volume density was calculated with Matlab for the particles from each sample. Additionally, the average volume diameter distribution was fitted with a log-NV distribution. A statistic report including the number mean diameter (NMD), the standard deviation related to the NMD and the parameters of the log-NV distribution was created. Figure 22 shows the histograms of a product sample for an exemplarily run from Exp S2 (V= 12.5 ml/min (PI) + 3.5 ml/min (PII), 7m reactor length).

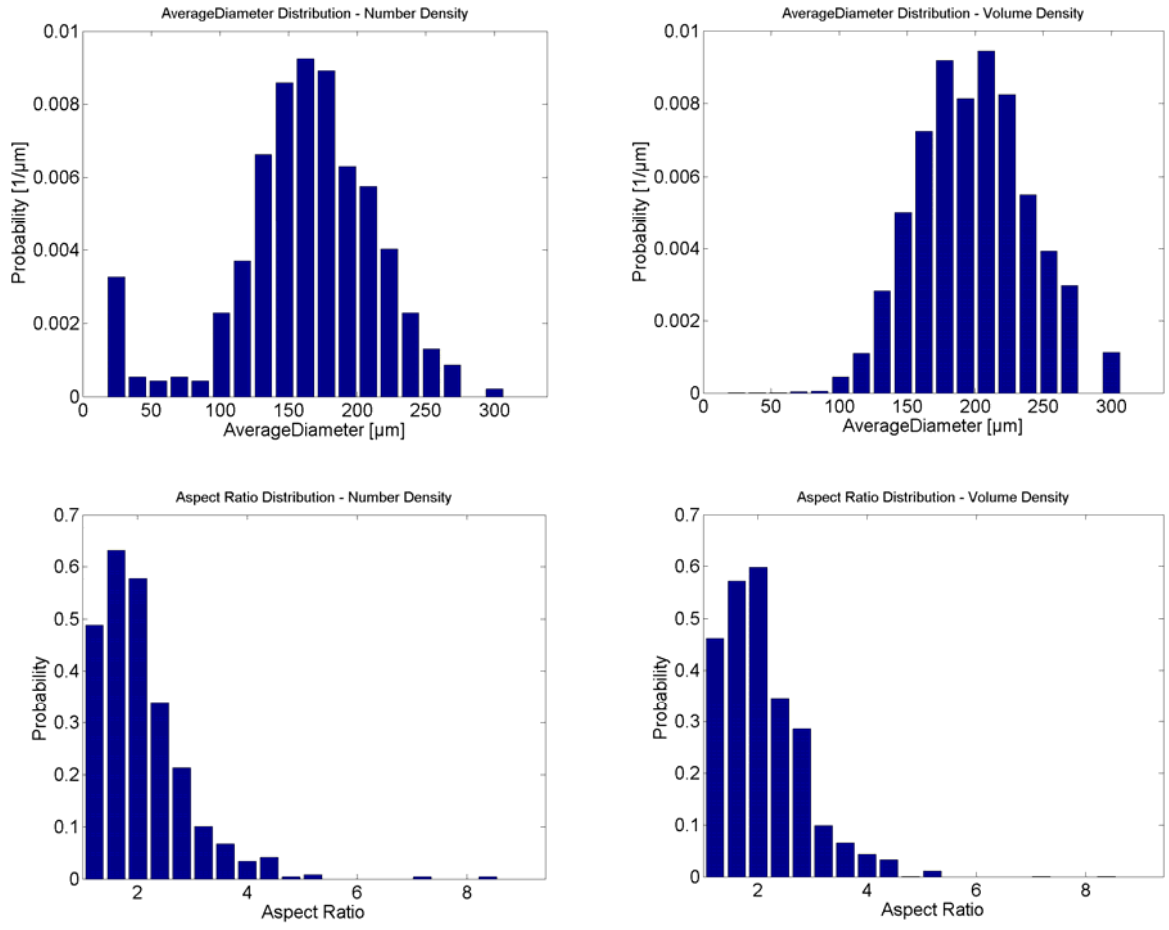

Figure 22: Top left-hand: Histogram of average diameter distribution (number density). Top right-hand: Histogram of average diameter distribution (volume density). Bottom left-hand: Aspect ratio distribution (number density). Bottom right-hand: Aspect ratio distribution (volume density)

Figure 23 shows the log-NV fit for the average diameter volume density shown in Figure 22. The log-NV fitting function was chosen because it gave a good characterization of the distribution, also regarding the amount of fines.

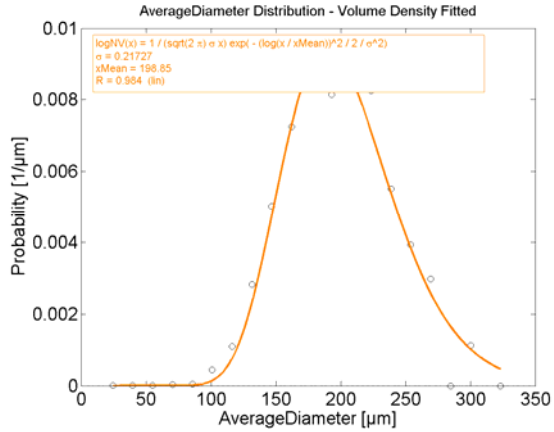

Figure 23: Histgram of log-NV fit of avarage diameter distribution

The average diameter and aspect ratio of the seed sample and two product samples of one run were compared to see any deviations. Figure 24 shows the graphical evaluation of the test run discussed above. The variation of the two product samples is not significant and probably due to statistical fluctuations.

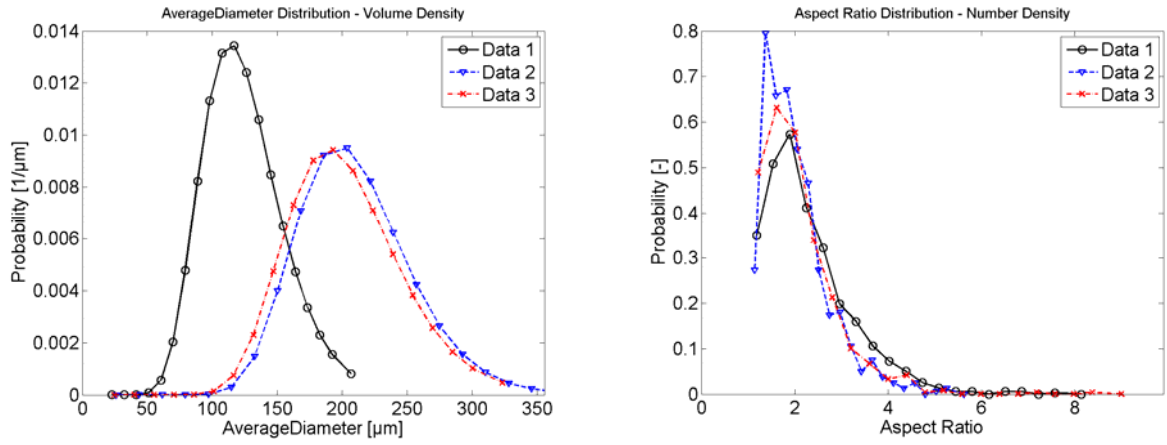

Figure 24: Comparison of seed and product samples of one test run (V= 12.5 (PI) + 3.5 ml/min (PII), 7m reactor length, Exp S2). Left-hand: Avarage diameter distribution for volume density (log-NV fit). Right-hand: Aspect ratio for number density

The CSD evaluation of experimental series Exp S1 is summarized in Table 4. The number mean diameter (NMD), the related standard deviation (s), the volume median diameter ($d_{p,50}$), and the related standard deviation (σ) are listed for every run. The increase of the NMD (ΔNMD) and the volume diameter ($\Delta d_{p,50}$) from the seed sample to an average value of product sample 2 and 3 are shown in Table 5.

Table 4: Mean diameter and standard deviation of number and volume density distribution of Exp S1 (a) + (b)

			7 m 11.4ml/min	10 m 11.4ml/min	15 m 11.4ml/min	15 m 17.4ml/min	15 m 23.4ml/min	(cool.) 15m 11.4ml/min
Seeds	NMD	µm	61.95	42.62	61.62	55.90	49.58	61.50
	s	µm	31.66	27.66	32.98	30.41	30.34	28.88
	$d_{p,50}$	µm	102.92	94.58	107.54	99.60	102.34	98.77
	σ	[-]	0.33	0.40	0.39	0.37	0.45	0.33
Probe 2	NMD	µm	131.40	95.77	139.59	95.56	73.40	133.94
	s	µm	75.62	75.41	76.20	72.39	65.30	95.85
	$d_{p,50}$	µm	222.06	227.61	227.23	202.84	204.99	251.99
	σ	[-]	0.26	0.29	0.34	0.28	0.25	0.21
Probe 3	NMD	µm	146.78	91.64	136.39	111.39	88.10	108.39
	s	µm	84.25	73.78	78.32	69.42	68.36	103.88
	$d_{p,50}$	µm	239.27	211.80	210.57	193.78	199.06	273.68
	σ	[-]	0.22	0.28	0.26	0.24	0.25	0.21

Table 5: ad evaluation Exp S1

		7 m 11.4ml/min	10 m 11.4ml/min	15 m 11.4ml/min	15 m 17.4ml/min	15 m 23.4ml/min	(cool.) 15m 11.4ml/min
NMD Seeds	µm	61.95	42.62	61.62	55.90	49.58	61.50
NMD (2.+3.)	µm	139.09	93.71	137.99	103.48	80.75	121.17
ΔNMD	µm	77.14	51.09	76.37	47.58	31.17	59.67
$d_{p,50}$ Seeds	µm	102.92	94.58	107.54	99.60	102.34	98.77
$d_{p,50}$ (2+3)	µm	230.67	219.71	218.90	198.31	202.03	262.84
$\Delta d_{p,50}$	µm	127.75	125.13	111.36	98.71	99.69	164.07

The summarized results of the CSD evaluation of experimental series Exp S2 listing the NMD, s, $d_{p,50}$, and σ for each run is shown in Table 6. Table 7 gives an overview of the NMD and $d_{p,50}$ increase for all runs.

Table 6: Mean diameter and standard deviation of number and volume density distribution of Exp S2

			3m 11.4ml/min	7m 11.4ml/min	10m 11.4ml/min	15m 11.4ml/min	15m 16 ml/min	15m 23 ml/min
Seeds	NMD	µm	115.12	79.65	89.5	87.59	80.56	85.41
	s	µm	47.40	30.86	34.14	30.50	31.95	29.48
	$d_{p,50}$	µm	165.05	112.05	126.35	114.65	115.53	111.48
	σ	[-]	0.31	0.29	0.29	0.26	0.30	0.28
Probe 2	NMD	µm	231.78	169.15	183.83	189.48	189.12	131.50
	s	µm	67.17	68.61	51.94	53.44	41.96	48.86
	$d_{p,50}$	µm	268.29	219.39	220.44	231.33	214.92	174.70
	σ	[-]	0.20	0.20	0.21	0.21	0.18	0.27
Probe 3	NMD	µm	219.84	180.03	169.19	204.06	180.60	137.45
	s	µm	55.12	69.43	44.42	55.26	45.36	44.77
	$d_{p,50}$	µm	255.04	230.02	198.73	244.02	212.14	174.58
	σ	[-]	0.20	0.20	0.19	0.22	0.20	0.25

Table 7: ad evaluation Exp S2

		3m 11.4ml/min	7m 11.4ml/min	10m 11.4ml/min	15m 11.4ml/min	15m 16 ml/min	15m 23 ml/min
NMD Seeds	µm	115.12	79.65	89.50	87.59	80.56	85.41
NMD (2.+3.)	µm	225.81	174.59	176.51	196.77	184.86	134.48
ΔNMD	µm	110.69	94.94	87.01	109.18	104.30	49.065
$d_{p,50}$ Seeds	µm	165.05	112.05	126.35	114.65	115.53	111.48
$d_{p,50}$ (2+3)	µm	261.67	224.71	209.59	237.68	213.53	174.64
$\Delta d_{p,50}$	µm	96.62	112.66	83.24	123.03	98.00	63.16

6.4. Flow Rate and Temperatures

The total volume flow through the reactor $\dot{V}_{tot}$ was the sum of the feed flow of solution 1 $\dot{V}_{F1}$ and the seed particle flow (suspension 2) $\dot{V}_{F2}$. Both flow rates could be adjusted independently due to two separate peristaltic pumps.

$$\dot{V}_{tot} = \dot{V}_{F1} + \dot{V}_{F2} \tag{6.13}$$

The reactor geometry was a cylindrical tube with the cross section area A_R calculated with the inner tube diameter d_i and the length L_R, which resulted in a total reactor volume of V_R.

$$A_R = \frac{d_i^2 \pi}{4} \tag{6.14}$$

$$V_R = A_R L_R \tag{6.15}$$

The flow velocity u was calculated based on the total volume flow related to the cross section area of the reactor.

$$u = \frac{\dot{V}_{tot}}{A_R} \tag{6.16}$$

The reactor volume divided by the total volume flow gives the residence time t_{res}. The residence time indicates how long the solution takes to pass the reactor.

$$t_{res} = \frac{V_R}{\dot{V}_{tot}} \tag{6.17}$$

The Reynolds number Re is a dimensionless number that indicates the ratio of inertial forces to viscous forces. It indicates if laminar or turbulent flow prevails inside the tube. The flow conditions influence local mixing and supersaturation, the heat transfer, and particle stress due to particle-particle and particle-wall interactions and shear stress. Laminar flow was observed for all runs due to the low flow rate and small inner tube diameter.

$$Re = \frac{u d_i \rho_{susp}}{\eta_{susp}} \tag{6.18}$$

The dynamic viscosity of the suspension η_{susp} was measured with a rheometer at 25 °C (Physica, Anton Paar, MCR 300). The density of the suspension ρ_{susp} was measured at the mixing point and the end of the reactor at different runs (see Appendix A.2). The parameters were interpolated according to the actual temperature.

The ASA-EtOH solution (1) experienced a strong temperature decrease due to cooling through air convection at room temperature while covering the distance of the PHARMED® tubing and the connection tubes when pumped from the storage vessel to the mixing piece (41 ±3 °C according to the flow rate). Still, no nucleation occurred before the solution was fed to the reactor, though the solution got close to the saturation limit at the end of the connection tube. After mixing the two inlet flows, the resulting suspension featured a temperature of 33 ±4 °C for Exp S1 (higher temperature for higher flow rates), and 37 ±5 °C for Exp S2.

Flow rate (u), residence time (t_{res}), storage temperature of feed solution 1 (T_{sol_1}) and seed suspension (T_{seeds}), room temperature (T_{room}), the temperature at the mixing point (T_M), and the temperature at the reactor end (T_E) from each experimental test are shown in Table 8 for Exp S1 and in Table 9 for Exp S2.

Table 8: Exp S1 - flow rates and temperatures

No.	L_R [m]	V_1 (P I) [ml/min]	V_2 (P II) [ml/min]	V_{total} [ml/min]	u [m/min]	t_{res} [s]	T_{room} [°C]	T_{sol_1} [°C]	T_{seeds} [°C]	T_M [°C]	T_E [°C]
1	7	8.9	2.5	11.4	3.63	116	21.1	62.0	21.1	29.3	23.8
2	10	8.9	2.5	11.4	3.63	165	21.1	62.0	21.1		24.3
3	15	8.9	2.5	11.4	3.63	248	22.3	62.0	22.3		
4	15	13	4.4	17.4	5.54	162	21.3	62.0	21.1	37.2	
5	15	18.4	5	23.4	7.45	121	21.3	62.0	21.3	33.5	

Table 9: Exp S2 - flow rates and temperatures

No.	L_R [m]	V_1 (P I) [ml/min]	V_2 (P II) [ml/min]	V_{total} [ml/min]	u [m/min]	t_{res} [s]	T_{room} [°C]	$T_{feed\ 1}$ [°C]	T_{seeds} [°C]	T_M [°C]	T_E [°C]
1	15	8.9	2.5	11.4	3.63	248	25.2	60.0	27.1	35.0	26.0
2	15	12	3.3	15.3	4.87	185	24.0	60.0	26.0	40.0	28.2
3	15	17.8	5.1	22.9	7.29	123	23.7	60.0	27.5	41.0	
4	15	25.8	7.5	33.3	10.60	85	21.7	60.0	26.4		
5	10	8.9	2.5	11.4	3.63	165	26.5	60.0	28.6	32.0	28.9
6	10	12.4	3.5	15.9	5.06	119	25.4	60.0	27.1	40.0	29.5
7	10	18	4.9	22.9	729	82	26.4	60.0	27.6	41.7	29.3
8	7	8.9	2.5	11.4	3.63	116	23.1	60.0	25.5	29.9	26.9
9	7	12.5	3.5	16.0	5.09	82	24.2	60.0	27.5	34.9	28.8
10	7	17.8	5	22.8	7.26	58	25.0	60.0	28.6	40.5	29.1
11	3	8.9	2.5	11.4	3.63	50	25.0	60.0	27.5		29.0
12	3	12.5	3.6	16.1	5.12	35	24.3	60.0	28.1	39.0	29.3
13	3	18	5.1	23.1	7.35	24	25.2	60.0	28.0	41.2	31.6

6.5. Mass Balance

A mass balance was done for the crystallizer to determine the mass fraction of solid ASA and the yield of the crystallization process. For this purpose the mass samples of the seed and product flow were evaluated. A mean value of the product samples was used to compare different runs. An evaluation regarding the consistency of samples of the same run proved that there was only a small deviation. There was no visible correlation of the deviation of mass to the order in which the samples were taken. Figure 25 shows a schematic of the mass balance for the reactor.

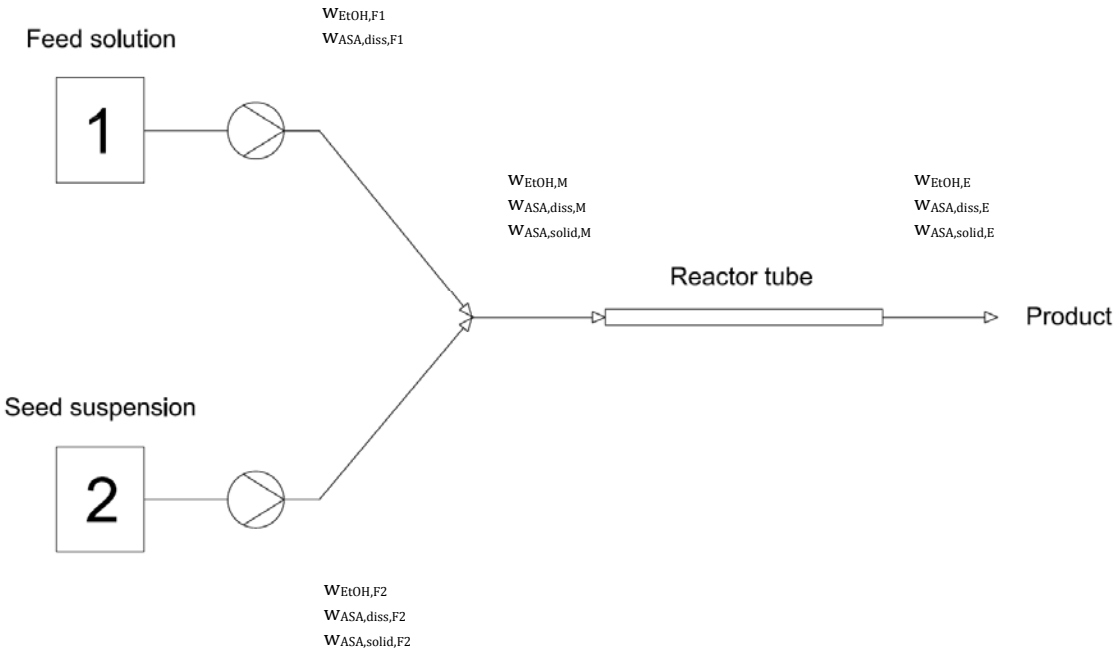

Figure 25: Mass balance over reactor

6.5.1. Experimental Data

For all experimental runs samples of the seed and product flow were taken and the mass of solid ASA was weighed. A summary of the data collected is given in Table 10 for Exp S1 (a) (air cooling) and Exp S1 (b) (intense cooling), and Table 11 for Exp S2 (constant temperature).

Table 10: Mass of ASA for seed and product samples for Exp S1 (a) (run no. 1-5) and Exp S1 (b) (run no. 6)

No.	L_R [m]	V_{total} [ml/min]	$m_{ASA,Seeds}$ [g/min]	$m_{ASA.Prod,Samp1}$ [g/min]	$t_{Sample1}$ [min]	$m_{ASA.Prod,Samp2}$ [g/min]	$t_{Sample2}$ [min]
1	15	11.4	0.3927	1.8323	5	1.8820	9
2	15	17.4	0.6014	2.4318	5	2.3681	10
3	15	23.4	0.7196	3.3075	5	3.1205	11
4	10	11.4	0.4027	1.7640	6	1.8093	10
5	7	11.4	0.3403	1.7818	4	1.4880	12
6	15	11.4	0.3422	2.4118	7	2.4266	11

Table 11: Mass of ASA for seed and product samples for Exp S2

No.	L_R [m]	V_{total} [ml/min]	$m_{ASA,Seeds}$ [g/min]	$m_{ASA.Prod,Samp1}$ [g/min]	$t_{Sample1}$ [min]	$m_{ASA.Prod,Samp2}$ [g/min]	$t_{Sample2}$ [min]
1	15	11.4	0.3282	1.1360	28	1.1132	33
2	15	15.3	0.4028	1.5650	20	1.4960	28
3	15	22.9	0.7415	2.6818	11	2.5744	16
4	15	33.3	0.9046	3.7444	5	3.9506	10
5	10	11.4	0.3373	1.1994	5	1.1680	8
6	10	15.9	0.5041	1.7082	4	1.6430	8
7	10	22.9	0.7076	2.4238	4	2.4520	7
8	7	11.4	0.3931	1.4536	12	1.3740	17
9	7	16	0.5523	1.5252	5	1.5956	10
10	7	22.8	0.7496	2.4302	4	2.4780	10
11	3	11.4	0.3080	1.5306	5	1.1776	10
12	3	16.1	0.3091	1.2758	5	1.2342	10
13	3	23.1	0.6028	2.3562	4	1.6644	10

6.5.2. Mass Flow of Feed Flows

The total mass flow $\dot{m}_{Fi}$ of each inlet flow was calculated according to the flow rate of each pump using the density of the suspension ρ_{susp}. The calculations noted above were performed for both solution and suspension flow respectively.

$$\dot{m}_{F1} = \dot{V}_{F1} \cdot \rho_{susp} \tag{6.19}$$

The mass fraction of each component w_i in the storage vessel was calculated considering the total mass of ASA $m_{ASA,Ii}$ and EtOH $m_{EtOH,Ii}$. It was assumed that a homogeneous solution/suspension of the same composition was fed to the reactor. The total mass flow of ASA $\dot{m}_{ASA,Fi}$ and EtOH $\dot{m}_{EtOH,Fi}$ of each flow was calculated by multiplying the mass fraction w_i with the total mass flow $\dot{m}_{Fi}$.

$$w_{ASA,F1} = \frac{m_{ASA,I1}}{m_{ASA,I1} + m_{EtOH,I1}} \tag{6.20}$$

$$\dot{m}_{ASA,F1} = \dot{m}_{F1} \cdot w_{ASA,F1} \tag{6.21}$$

$$\dot{m}_{F1} = \dot{m}_{ASA,F1} + \dot{m}_{EtOH,F1} \tag{6.22}$$

6.5.3. Saturation Calculation with Nyvlt Model

The solubility of ASA in ethanol was calculated according to the Nyvlt model using the parameters N_1-N_3 established in [20]. x_{ASA} is the maximum mole fraction of ASA that is soluble in EtOH at the temperature T [K].

$$\log(x_{ASA,sat}) = N_1 + \frac{N_2}{T} + N_3 \log(T) \tag{6.23}$$

Nyvlt parameters: $N_1 = 27.769$

$N_2 = -2500.906$

$N_3 = -8.323$

The theoretical seed particle load $\dot{m}_{ASA,solid(Nyvlt)}$ was calculated considering the difference Δx of the actual ASA concentration x_{ASA} to the saturation concentration according to Nyvlt $x_{ASA,sat}$.

$$\Delta x = x_{ASA} - x_{ASA,sat} \tag{6.24}$$

$$\dot{n}_{ASA,solid(Nyvlt)} = \Delta x \cdot \dot{n}_{ASA,F2} \tag{6.25}$$

For the saturation calculation equation according to Nyvlt the concentration was given as mole fraction. Therefore it had to be converted to mass fraction for further calculations.

$$\dot{m}_{ASA,solid(Nyvlt)} = \dot{n}_{ASA,solid(Nyvlt)} \cdot MW_{ASA} \tag{6.26}$$

6.5.4. Total Mass Flow

The sum of both feed solution and seed suspension flow resulted in the total mass flow $\dot{m}_{tot}$ through the reactor.

$$\dot{m}_{tot} = \dot{m}_{F1} + \dot{m}_{F2} \tag{6.27}$$

The total mass flow of ASA $\dot{m}_{ASA,M}$ considered the mass of both dissolved ASA $\dot{m}_{ASA,diss,M}$ and solid ASA $\dot{m}_{ASA,solid,M}$ of the mixture of feed solution and seed suspension at the reactor inlet with a related mass fraction of ASA $w_{ASA,M}$.

$$\dot{m}_{ASA,M} = \dot{m}_{ASA,F1} + \dot{m}_{ASA,F2} \tag{6.28}$$

$$\dot{m}_{ASA,M} = \dot{m}_{ASA,solid,M} + \dot{m}_{ASA,diss,M} \tag{6.29}$$

$$\dot{m}_{EtOH,M} = \dot{m}_{tot} - \dot{m}_{ASA,M} \tag{6.30}$$

$$w_{ASA,M} = \frac{\dot{m}_{ASA,M}}{\dot{m}_{tot}} \tag{6.31}$$

$$w_{EtOH,M} = 1 - w_{ASA,M} \tag{6.32}$$

The assumption was made that during the mixing of the two feed flows no nucleation took place. Accordingly, the mass fraction of seed particles at the reactor inlet was therefore calculated considering the mass of solid ASA of the seed suspension $\dot{m}_{ASA,solid,F2}$ and referred to the total mass flow.

$$w_{ASA,solid,M} = \frac{\dot{m}_{ASA,solid,F2}}{\dot{m}_{tot}} \qquad \textit{mass fraction of seed particles} \tag{6.33}$$

6.5.5. Results Mass Gain

The average mass flow of the product $\dot{m}_{ASA,Prod}$ was calculated as an average value of sample 2 and 3. The overall mass increase of the product particles $\Delta\dot{m}_{ASA,Solid}$ was calculated as the difference of solid ASA in the seed sample to the product sample. Δm indicates the percentage mass increase of solid ASA (yield). For Exp S2 the theoretical mass of solid ASA according to Nyvlt regarding supersaturation was calculated.

$$\Delta\dot{m}_{ASA,Solid} = \dot{m}_{ASA,Prod} - \dot{m}_{ASA,Seeds} \tag{6.34}$$

$$\Delta m = \frac{\Delta m_{ASA,solid}}{\dot{m}_{ASA,solid,F2}} 100\% \tag{6.35}$$

The mass of the seed sample $\dot{m}_{ASA,Seeds}$ and an average value of the product sample $\dot{m}_{ASA,Prod}$ from each run are shown together with the mass increase $\Delta\dot{m}_{ASA,Prod}$ of the particles and the yield Δm in Table 12 for Exp S1 and Table 13 for Exp S2. Additionally, the theoretical mass of solid ASA according to the Nyvlt model was calculated for Exp S2

Table 12: Mass gain Exp S1

Run No.	L_R [m]	V_{tot} [ml/min]	$m_{ASA,Seeds}$ [g/min]	$m_{ASA,Prod}$ [g/min]	$\Delta m_{ASA,Solid}$ [g/min]	Δm [%]	
1	15	11.4	0.3927	1.8572	1.4645	373	
2	15	17.4	0.6014	2.4000	1.7986	299	
3	15	23.4	0.7196	3.2140	2.4944	347	
4	10	11.4	0.4027	1.7867	1.3840	344	
5	7	11.4	0.3403	1.6349	1.2946	380	
6	15	11.4	0.3422	2.5003	2.1581	631	+ extra cooling

Table 13: Mass gain Exp S2

Run No.	L_R [m]	V_{tot} [ml/min]	$m_{ASA,Seeds}$ [g/min]	$m_{ASA,Prod}$ [g/min]	$\Delta m_{Partikel}$ [g/min]	Δm [%]	$m_{Seeds(Nyvlt)}$ [g/min]	$m_{Prod(Nyvlt)}$ [g/min]
1	15	11.4	0.3282	1.2376	0.8341	254.1	0.3420	1.5081
2	15	15.3	0.4028	1.6493	1.2465	309.5	0.4726	2.1324
3	15	22.9	0.7415	2.6281	1.8866	254.4	0.7043	3.1954
4	15	33.3	0.9046	3.8475	2.9429	325.3		
5	10	11.4	0.3373	1.1837	0.8464	250.9	0.3223	1.4171
6	10	15.9	0.5041	1.6503	1.1462	227.4	0.4726	2.0842
7	10	22.9	0.7076	2.4146	1.7070	241.2	0.6335	2.8272
8	7	11.4	0.3931	1.4138	1.0207	259.7	0.3700	1.6353
9	7	16.0	0.5523	1.5891	1.0368	187.7	0.4974	2.2443
10	7	22.8	0.7496	2.5032	1.7536	233.9	0.6636	3.0435
11	3	11.4	0.3080	1.2531	0.9451	306.9	0.3391	1.5150
12	3	16.1	0.3091	1.2252	0.9161	296.4	0.4933	2.2451
13	3	23.1	0.6028	2.0103	1.4075	233.5	0.6620	3.0143

Only the difference of the absolute masses was assessed. To describe the mass increase of single crystals inside the reactor a population balance would be necessary. A population balance describes nucleation and crystal growth during a crystallization process considering birth and death rate, breakage and agglomeration of particles. Various publications like [25-29] discuss this topic for continuous crystallization. However, due to the complexity of factors influencing crystallization processes [3], adjusting a model for the application presented in this work would have exceeded the extent of this thesis.

7. Result Discussion

7.1. PSD and NMD

The particle size distribution (PSD) of seed and product samples was compared for each test run and subsequently the runs were compared among one another.

For experimental series Exp S1 the seed particles featured an average volume diameter distribution in the range of 20-250 ±30 µm, an average volume diameter of 100 µm and average NMD of 55 µm. The seed particles of Exp S2 were in the range of 50-230 ±30 µm, featuring a mean volume diameter of 115 µm and an average NMD of 85 µm. A comparison of test runs from Exp S2 (Figure 26) with a constant reactor length of 15 m and three different flow rates showed a steady product PSD range of 300 ±30 µm (volume diameter) that shifted to smaller particle sizes with increased flow rate. Runs from Exp S1 however did not show a significant variation of the volume density distribution, although a clear decrease of the NMD was observed as in Exp S2.

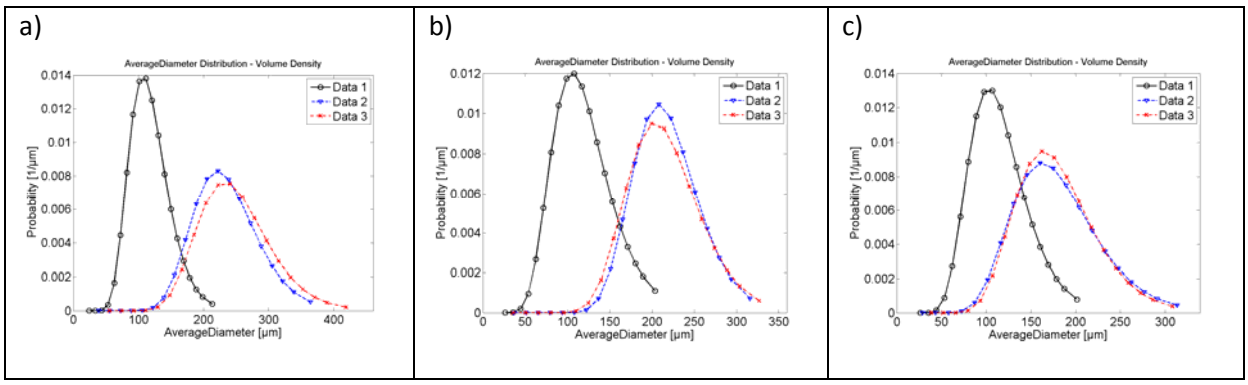

Figure 26: Comparision of the PSD for constant reactor length (15m) and varying flow rate for a constant temperature of 30°C (Exp S2) [Data 1 = seed sample, Data 2 = product sample 2, Data 3= product sample 3]. a) Run with a total flow rate of V_{tot} = 11.4 ml/min. b) Run with V_{tot} = 15.3 ml/min. c) Run with V_{tot} = 22.9 ml/min.

The PSD for test runs of Exp S2 with constant flow rate ranged from 130-400 ±40 µm (volume diameter). No significant change of the product PSD was observed for varying reactor lengths. The same applied for runs of Exp S1.

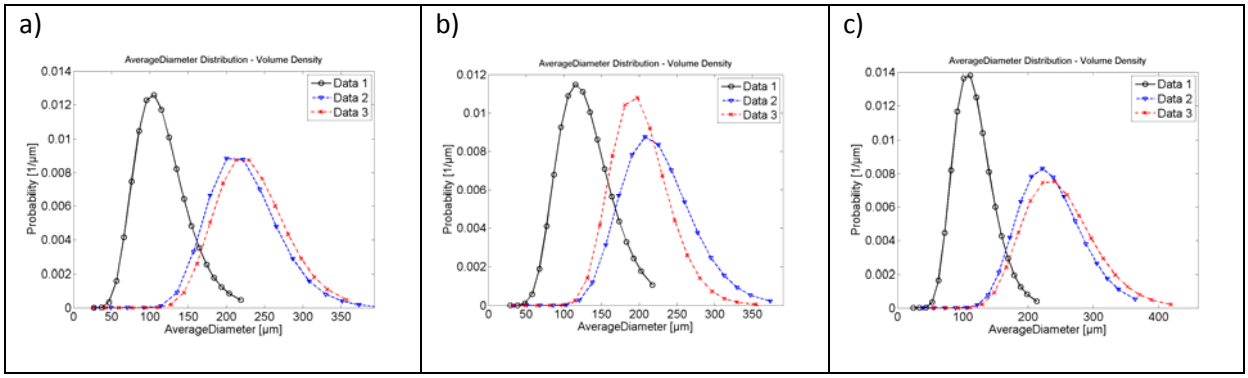

Figure 27: Comparision of the PSD for a constant flow rate of V_{tot}= 11.4 ml/min and varying reactor length for a constant temperature of 30°C (Exp S2). [Data 1 = seed sample, Data 2 = product sample 2, Data 3= product sample 3]. a) Run with a reactor length of 7 m. b) Run with a reactor length of 10 m. c) Run with a reactor length of 15 m

Figure 27 shows a comparison of three exemplarily runs from Exp S2 with a constant flow rate of 11.4 ml/min and varying reactor length. The aspect ratio distribution of the product particles featured a narrower distribution than the one for seed particles. The seed particles of both Exp S1 and Exp S2 featured an aspect ratio of 1-8, the product particles of 1-6. The aspect ratio was not observed specifically in the sample evaluation. Figure 28 shows an exemplary comparison of the aspect ratio number distribution of product and seed samples.

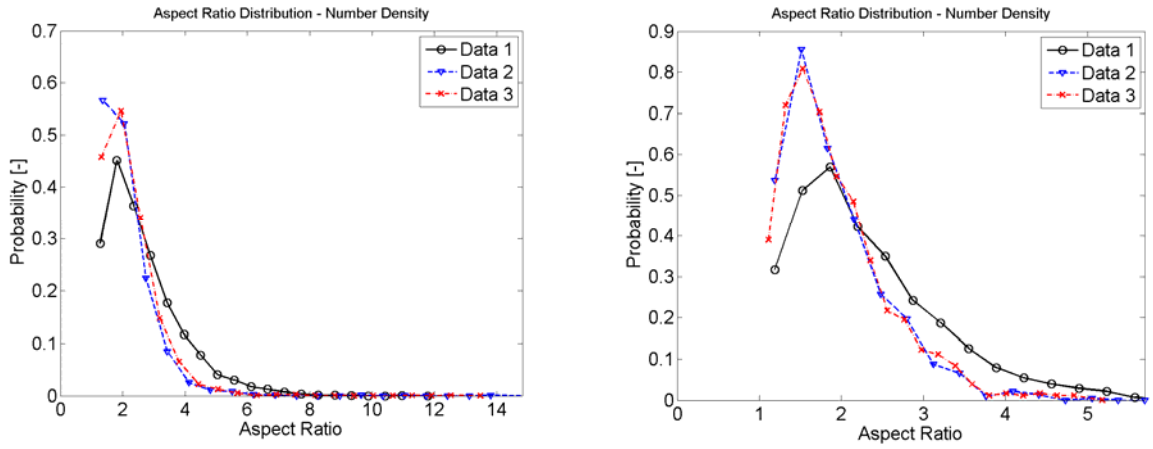

Figure 28: Aspect ratio distribution of seed and product samples for a run with V= 17.8 ml/min (PI) + 5 ml/min (PII), 7m reactor length. [Data 1 = seed sample, Data 2 = product sample 2, Data 3= product sample 3]. Left-hand: Results achieved with air cooling (Exp S1). Right hand: Results achieved with constant temperature (Exp S2)

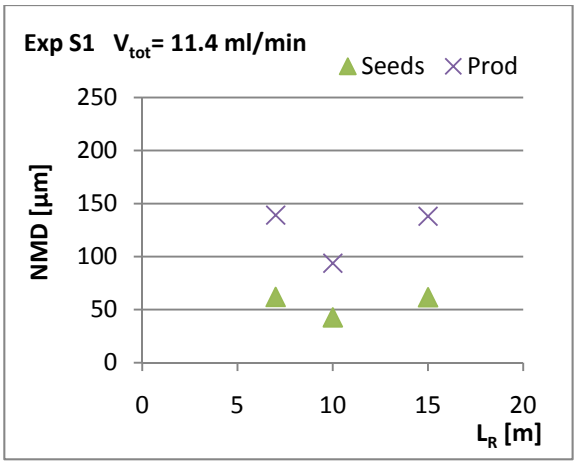

Figure 29: Exp S1 – NMD vs reactor length

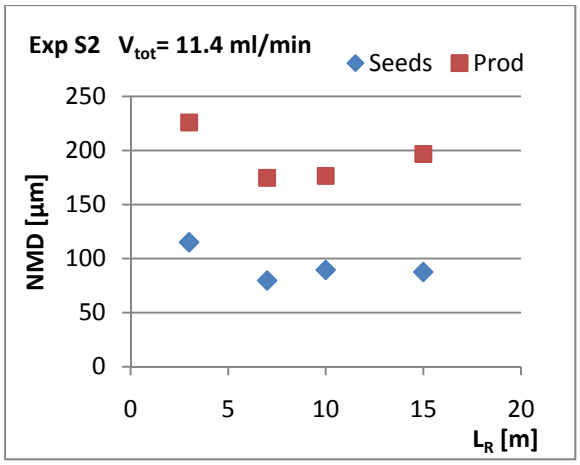

Figure 30: Exp S2 – NMD vs reactor length

The NMD of seed and product particles was assessed for a constant flow rate of 11.4 ml/min with varying reactor lengths. Although a clear increase of the NMD from seed to product particles was noted in both Exp S1 (Figure 29) and Exp S2 (Figure 30), there was no significant change of the NMD considering different reactor lengths. The residence time of 116-248 sec was in general rather short for a crystallization process and such small variations did not have a visible effect on the product outcome. However, a stronger increase of the NMD for Exp S2 that was kept at a constant temperature of 30 °C in comparison to Exp S1 that was cooled with air at room temperature (21 °C) was noted, as is shown in Figure 31. The temperature gradient clearly affected the resulting NMD.

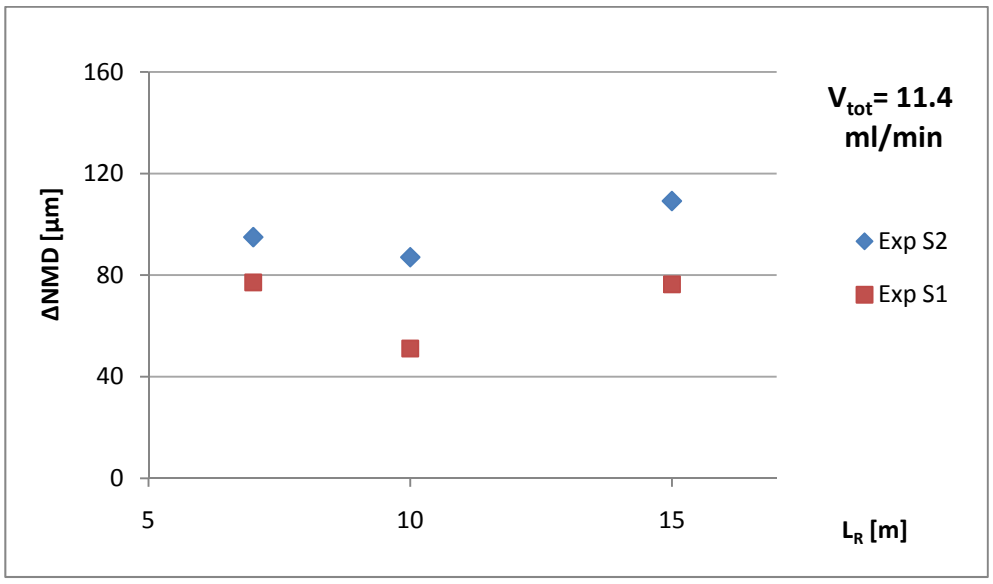

Figure 31: Increase of NMD due to variation of reactor length

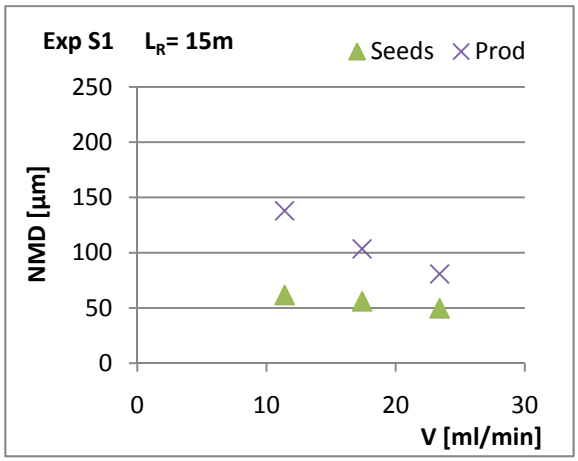

Figure 32: Exp S1 – NMD vs flow rate

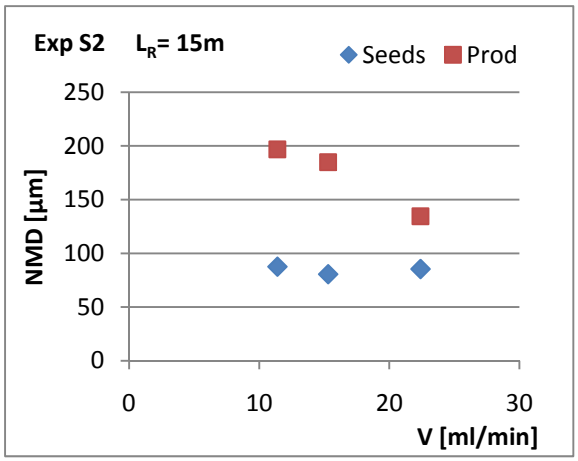

Figure 33: Exp S2 – NMD vs flow rate

Figure 32 and Figure 33 show that the NMD of the product flow decreases with increasing flow rate in both Exp S1 and Exp S2. This aspect most likely is related to increased shear stress for higher flow rates, and therefore reduced agglomeration. It was presumed that longer residence times would lead to increased crystal growth, but as test runs with varying reactor length had shown, the overall residence time was rather short for all runs and therefore no significant changes of the crystal size were observed. Figure 34 shows that the overall increase of the NMD for varying flow rate was higher in Exp S2 than in Exp S1.

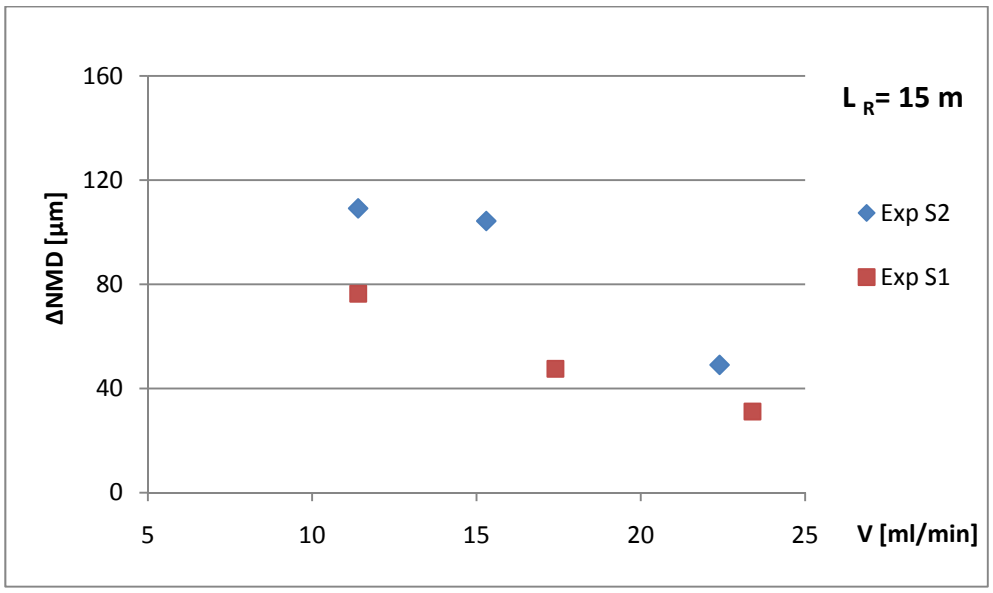

Figure 34: Increase of NMD due to variation of flow rate

7.2. Mass Gain

Figure 35 shows the total mass increase Δm_{tot} from seed to product particles for different flow rates and reactor lengths. A linear increase of the total mass-throughput is related to higher flow rates. The mass increase of the particles with the same flow rate did not change significantly with increased reactor length, nor did increased flow rates produce a higher yield. Given the fact that the NMD of the product crystals decreased with increased flow rate but the total mass output of solid ASA remained the same, the amount of particles at the end of the reactor must be higher, probably due to reduced agglomeration. No considerable effect of the residence time on the particle growth was observed, but this might be related to too narrow time intervals, as discussed previously in chapter 7.1.

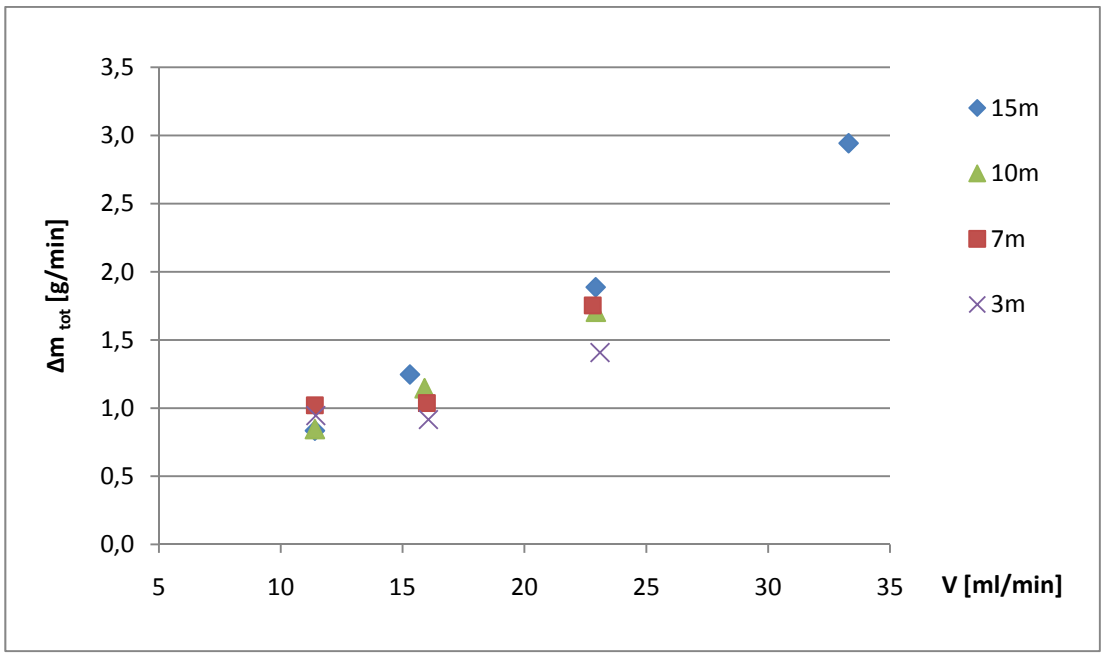

Figure 35: Total mass increase of the particles for different reactor lengths and for varying flow rates (Exp S2)

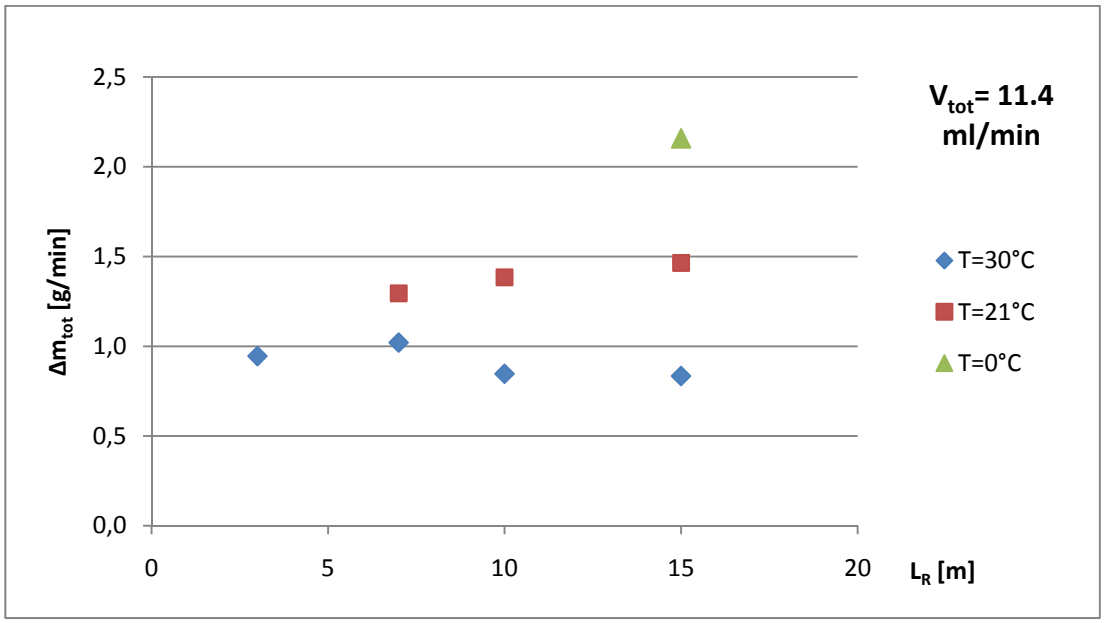

Figure 36: Influence of different cooling rates on the particle mass gain

The influence of different cooling rates on the particle mass gain is shown in Figure 36. Three runs with a constant flow rate of 11.4 ml/min but different cooling methods are compared. T indicates the temperature at the reactor outlet. The blue series (Exp S2) was completed with a constant temperature of 30 °C throughout the entire crystallization process, the red series (Exp S1) with air cooling at room temperature, and the green measurement (Exp S1 (b)) with different cooling steps and a final solution temperature of 0 °C. A considerable increase of product mass gain with decreasing solution temperature was observed by comparing the runs with T= 30 °C and T= 21 °C. A further notable mass increase was observed for the run with intense cooling, but did not exceed the expectations, considering the mass gain achieved with a rather small temperature difference between run 1 and 2.

However, more test runs would be necessary for a more accurate analysis on how temperature gradients influence the product outcome.

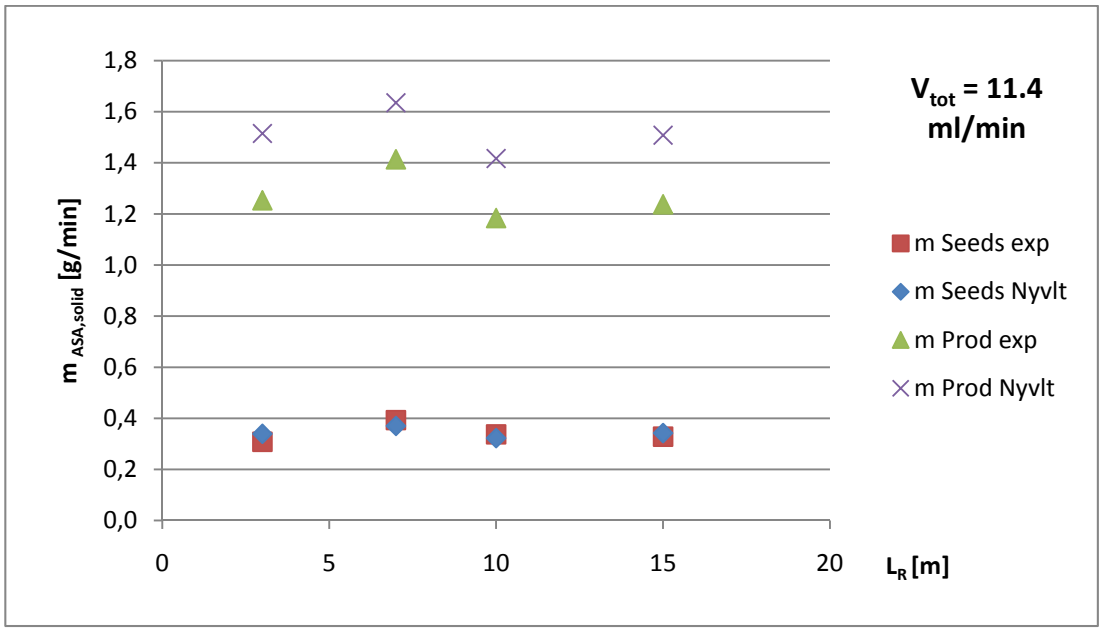

Figure 37: Mass of particles measured compared to mass calculated using Nyvlt saturation concentration (Exp S2)

Figure 37 shows a comparison of the measured mass of solid ASA of the seed feed and the theoretical mass of undissolved ASA considering only the saturation concentration calculated with Nyvlt parameters according to equation (6.23).

The calculated values match the measured masses very accurately for the seed feed. This proves that the solution was in equilibrium when fed into the reactor and the correlation between the saturation limit and the mass dissolved was confirmed. The mass of the product flow was also compared to the possible mass output by only considering the saturation limit. The product mass flow remained clearly under the calculated value, however, the deviation from calculated to measured mass was the same for all runs. A possible explanation would be that the residence time was not sufficient for further crystal growth and reaching thermodynamical equilibrium, as discussed for Figure 35.

8. Conclusion and Outlook

Summary of achievements:

- Design of a basic reactor concept
- Development of an experimental approach
- Testing of the system under varying process conditions
- Implementation of evaluation tools

A seeded tubular crystallizer was successfully designed and operated. Even though the system proved to be sensitive to inaccurate or interrupted dosing of the inlet flows and eventual stagnation areas in junction pieces, the experimenters were able to adapt the system for any desired adjustment and run the crystallization process in a stable way.

The system was tested for different process conditions. An experimental series Exp S1 (a) investigated the influence of varying reactor lengths and flow rates for a low cooling gradient through air convection at room temperature (21 °C). Additionally, in experimental series Exp S1 (b) intense cooling through multiple cooling segments (water baths, up to 0 °C) was applied. The influence of varying reactor lengths and flow rates for constant temperature (water bath, 30 °C) was investigated in experimental series Exp S2.

Higher flow rates led to increased shear stress and increased particle-particle interactions resulting in less agglomeration, and therefore smaller NMDs of the product crystals. The overall product mass however remained the same, suggesting the presence of a larger number of smaller particles. Different reactor lengths were applied to change the residence time while keeping the flow parameters constant. In both experimental series no significant change of the NMD and no increase of the yield was observed, most likely because the residence times were generally short for crystallization processes. The product mass to seed ratio was increased considerably by applying air cooling at room temperature compared to the runs with constant temperature of 30 °C. Intense cooling due to different cooling segments with a reactor end temperature of 0 °C resulted in further increase of the yield.

The comparison of different samples taken after different time intervals showed only minor variations. Steady state status was reached very quickly inside the reactor tube. Preliminary tests showed that the material of the tube and the fitting angle had an influence on the nucleation behavior, and therefore on the operability of the reactor. Too steep cooling profiles created excessive supersaturation and resulted in strong primary nucleation, and consequently plugging of the reactor tube. To achieve an optimum crystallization progression, the saturation level of the solution inside the reactor should be kept constant during the whole crystallization process. This could be accomplished by adapting the cooling steps, preferably starting with a small temperature gradient and proceeding with increased (stronger) cooling.

Although the aim was to develop and implement a continuously operated crystallizer, the reactor was run in a semi-continuously operating mode due to batch-wise preparation of seed particles and feed solution. As a final step to realize a real continuously operated system, the seed generation has to be fully integrated in the crystallization process. Implementing the seed production into the process would ensure a constant seed particle feed into the reactor, avoiding mixing issues related to different fill levels in the storage vessel, and deviations from batch to batch. This could be done by implementing a recycle flow with product classification (e.g. fines trap) combined with a size reduction step (e.g. ultrasonic irradiation). A recycle flow would also reduce solvent consumption, waste, and costs. Continuous production of feed solution and seed suspension would enable to operate the reactor for a longer time period while granting the same initial conditions.

As a next step in the reactor development, further tests regarding different cooling gradients should be scheduled as the temperature progression throughout the crystallization process seemed to influence the product yield most. The impact of different seed load should also be assessed, as this factor has not been considered much so far. An evaluation of the overall plant efficiency should be done to validate different cooling methods and operation steps. The sample analysis done with the microscope has proved to be reliable but should be replaced by an evaluation method that requires less time and effort like an automated particle characterization system (e.g. Quicpic (Sympatec) or Morphologi G3 (Malvern)).

9. References

[1] B. Y. Shekunov, P. Chattopadhyay, H. H. Y. Tong, A. H. L. Chow, “Particle Size Analysis in Pharmaceutics: Principles, Methods and Applications,” *Pharmaceutical Research*, vol. 24, Feb. 2007, S. 203-227.

[2] B. Y. Shekunov, P. York, “Crystallization processes in pharmaceutical technology and drug delivery design,” *Journal of Crystal Growth*, vol. 211, 2000, S. 122-136.

[3] K. Chow, H. H. Y. Tong, S. Lum, A. H. Chow, “Engineering of pharmaceutical materials: An industrial perspective,” *Journal of Pharmaceutical Sciences*, vol. 97, Aug. 2008, S. 2855-2877.

[4] N. Variankaval, A. S. Cote, M. F. Doherty, “From Form to Function: Crystallization of Active Pharmaceutical Ingredients,” *AIChE Journal*, vol. 54, Juli. 2008, S. 1682-1688.

[5] A. Pellek, P. Van Arnum, “Continuous Processing: Moving with or against the Manufacturing Flow,” *Pharmaceutical Technology*, vol. 9, Sep. 2008, S. 52-58.

[6] Allan S. Myerson, *Handbook of Industrial Crystallization*, Butterworth-Heinemann, 2002.

[7] T. Crosby, “Designing For the Future of Continuous Processing,” 2006.

[8] S. Lawton, G. Steele, P. Shering, L. Zhao, I. Laird, X.-W. Ni, “Continuous Crystallization of Pharmaceuticals Using a Continuous Oscillatory Baffled Crystallizer,” *Organic Process Research & Developement*, vol. 13, 2009, S. 1357-1363.

[9] G. Tekautz, “Überblick zur Partikel-Herstellung in Mikroreaktoren,” Microinnova, 2008.

[10] W. Ehrfeld, V. Hessel, H. Löwe, *Microreactors*, Weinheim: WILEY-VCH, 2000.

[11] P. Watts, S. J. Haswell, “Continuous flow reactors for drug discovery,” *Drug Discovery Today*, vol. 8, Juli. 2003, S. 586-593.

[12] A. S. Myerson, “Molecular crystals of controlled size,” U.S. Patent US 0030170999.

[13] R. D. Dombrowski, J. D. Litster, N. J. Wagner, Y. He, “Crystallization of alpha-lactose monohydrate in a drop-based microfluidic crystallizer,” *Chemical Engineering Science*, vol. 62, Mai. 2007, S. 4802-4810.

[14] C. J. Gerdts, V. Tereshko, M. K. Yadav, I. Dementieva, F. Collart, A. Joachimiak, R. C. Stevens, P. Kuhn, A. Kossiakov, R. F. Ismagilov, "Time-controlled microfluidic seeding in nL-volume droplets to separate nucleation and growth stages of protein crystallization," *Angewandte Chemie - International Edition*, vol. 45, 2006, S. 8156-8160.

[15] V. Hessel, H. Löwe, "Microreactor Technology: Applications in Pharma/Chemical Processing," *Innovations in Pharmaceutical Technology*, Feb. 2005, S. 88-92.

[16] R. Gray, Syrris Ltd, "Microreactors - A New Technology for Pharma Chemistry," *Innovations in Pharmaceutical Technology*, vol. 16, März. 2005, S. 90-93.

[17] E. L. Paul, H.- H. Tsung, M. Midler, "Organic crystallization processes," *Powder Technology*, 2005, S. 133-143.

[18] A. Mersmann, *Crystallization Technology Handbook*, New York: Marcel Dekker, 1995.

[19] A. Mersmann, M. Kind, J. Stichlmair, *Thermische Verfahrenstechnik - Grundlagen und Methoden*, Berlin Heidelberg: Springer, 2005.

[20] G. D. Maia, M. Giulietti, "Solubility of Acetylsalicylic Acid in Ethanol, Acetone, Propylene Glycol, and 2-Propanol," *Journal of Chemical & Engineering Data*, vol. 53, 2008, S. 256-258.

[21] E. Miyasaka, Y. Kato, M. Hagisawa, I. Hirasawa, "Effect of ultrasonic irradiation on the number of acetylsalicylic acid crystals produced under the supersaturated condition and ability of controlling the final crystal size via primary nucleation," *Journal of Crystal Growth*, vol. 289, 2006, S. 324-330.

[22] R. Neuper, F. Mayrhuber, G. Krammer, G. Aichinger, *Skriptum zu LV 352.001 Mechanische Verfahrenstechnik VO*, Institut für Apparatebau, Mechanische Verfahrenstechnik und Feuerungstechnik, TU Graz, 2002.

[23] W. S. Rasband, *ImageJ Documentation*, U.S. National Institutes of Health, Bethesda, Maryland, USA, 2009.

[24] J. Garside, A. Mersmann, J. Nyvlt, *Measurement of Crystal Growth and Nucleation Rates*, Rugby, UK: IChemE, 2002.

[25] J. Raasch, A. Wulf, *Statistik für Verfahrenstechniker und Chemie-Ingenieure*, Karlsruhe: 2010.

[26] H. Gros, T. Kilpiö, J. Nurmi, “Continuous cooling crystallization from solution,” *Powder Technology*, 2001, S. 106-115.

[27] A. J. Alvarez, A. S. Myerson, “Continuous Plug Flow Crystallization of Pharmaceutical Compounds,” *Crystal Growth & Design*, vol. 10, 2010, S. 2219-2228.

[28] C. Lindenberg, M. Krättli, J. Cornel, M. Mazotti, J. Brozio, “Design and Optimization of a Combined Cooling/Antisolvent Crystallization Process,” *Crystal Growth & Design*, vol. 9, 2009, S. 1124-1136.

[29] A. Gerstlauer, S. Motz, A. Mitrovic, E.-D. Gilles, “Development, analysis and validation of population models for continuous and batch crystallizers,” *Chemical Engineering Science*, vol. 57, 2002, S. 4311-4327.

[30] S. M. Nowee, A. Abbas, J. A. Romagnoli, “Optimization in seeded cooling crystallization: A parameter estimation and dynamic optimization study,” *Chemical Engineering and Processing*, vol. 46, 2007, S. 1096-1106.

[31] *ChemDAT, Merck Chemiedatenbank*, 2007.

[32] *VDI-Wärmeatlas online Ausgabe*, Berlin Heidelberg: Springer Verlag, 2006.

Appendix

A.1. Substances

Table 14: List of substances used during experiments

Material	Manufacturer
Acetylsalicylic acid (99.9%)	Sigma Life Science
Ethanol (98.9%, denaturized with 1.0% MEK)	Lactan, Roth
Cyclohexan	Lactan, Roth
Deionized water	

The material parameters for the chemicals in use were taken from different public databases. The density and dynamic viscosity of the solution at different temperatures was measured repeatedly after the Y-junction and the reactor outlet.

Table 15: Measured thermophysical parameters of suspension

T [K]	ρ [kg/m^3]	η [Pa*s]
273.15	940	0.8
299.15	926	0.61
303.15	910	0.6
313.15	900	0.5
333.15	884	0.4

Table 16: Material properties of ASA [31]

MW	=	180.15	[g/mol]
ρ	=	1350	[kg/m3]
Δh_{cryst}	=	1.65*10^5	[J/kg]

Table 17: Thermophysical properties of EtOH [32]

MW = 46.07 [g/mol]

T [K]	ρ [kg/m^3]	η [Pa*s]	c_p [J/(kg*K)]	λ [W/(m*K)]
273.15	808.6	1.77E-03	2.253	0.175
293.15	791.7	1.18E-03	2.398	0.169
323.15	764.5	6.90E-04	2.673	0.162
373.15	712.6	3.20E-04	3.304	0.155

Table 18: Thermophysical properties of water [32]

MW = 18.02 [g/mol]

T [K]	ρ [kg/m^3]	η [Pa*s]	c_p [J/(kg*K)]	λ [W/(m*K)]	h [kJ/kg]	Pr [-]
273.15	999.84	1.73E-03	4.219	0.562	0.0597	13.45
283.15	999.70	1.31E-03	4.195	0.582	42.117	9.414
293.15	998.21	1.00E-03	4.185	0.600	84.012	6.991
303.15	995.65	7.97E-04	4.180	0.615	125.83	5.419
313.15	992.22	6.35E-04	4.179	0.629	167.62	4.341
323.15	988.05	5.47E-04	4.180	0.641	209.41	3.568
333.15	983.21	4.66E-04	4.183	0.651	251.22	2.998
343.15	977.78	4.04E-04	4.188	0.660	293.07	2.565

Table 19: Thermophysical properties of air [32]

MW = 28.97 [g/mol]

T [K]	ρ [kg/m^3]	η [Pa*s]	c_p [J/(kg*K)]	λ [W/(m*K)]	h [kJ/kg]	Pr [-]
273.15	1.2758	1.72E-05	1.0059	2.44E-02	-25.15	0.711
283.15	1.2306	1.77E-05	1.0061	2.51E-02	-15.09	0.7095
293.15	1.1885	1.82E-05	1.0064	2.59E-02	-5.03	0.7081
303.15	1.1492	1.87E-05	1.0067	2.66E-02	5.04	0.7068
313.15	1.1124	1.92E-05	1.0071	2.74E-02	15.11	0.7056
323.15	1.0779	1.96E-05	1.0077	2.81E-02	25.18	0.7045

A.2. Equipment

Table 20: Equipment list

Component	Specifications	Description
Reactor tube	d_i= 2.0mm, d_a= 4.0mm	Polysiloxane tubing
Pump I	Ismatec BVP-Process IP 65 – 3/6	For ASA-EtOH solution (1)
Pump II	Ismatec RegloDigital MS2/6 V1.13C	For seed suspension (2)
Pump tubing I	d_i= 1.6mm, d_o= 4.8mm, L=0.4m	Pharmed® tubing
Pump tubing II	d_i= 2.79mm, d_o= 5.0mm,L=0.4m	Pharmed® tubing
Connection tubing 1	d_i= 2.0mm, d_o= 4.0mm, L= 0.2m	Polysiloxane, storage to pump
Connection tubing 2	d_i= 2.0mm, d_o= 4.0mm, L= 1.4m	Polysiloxane, pump to Y-fitting
Junction pieces	d_i= 2.0mm	PTFE, T- and Y-shape
Storage tank 1	V = 2L	For ASA-EtOH solution (1)
Storage tank 2	V = 2L	For seed suspension (2)
Plastic tube	d_o= 80mm, L= 0.1m	PP, to coil reactor tube
Bended metal frame	d_o= 0.1m, L= 0.25m	Aluminum, to coil reactor tube
Water bath 1	Heating bath, LxBxH= 30x20x20cm	For ASA-EtOH solution (1)
Water bath 2	Heating bath, LxBxH= 50x30x14cm	For reactor tube (Exp S2)
Water bath 3-6	varying	For additional cooling segments
Water bath UI	LxBxH= 25x12x10cm	For ultrasonic irradiation
Thermometer 1	Testo 110	For water baths
Thermometer 2	Fluke 50 D	For solution and suspension
Thermometer 3	Stem thermometer	For water bath 1
Blade stirrer	L_{Blade}= 40mm	For ASA-EtOH solution (1)
Magnetic stirrer	Standard device	For seed suspension (2)
Suction strainer	d = 50mm, glass material	For sampling
Filter	d = 80mm	For sampling
Water jet pump	Standard device	For sampling
Microscope	Laica DM 4000	For sample analysis
Digital camera	Laica DFC 290	For sample analysis